DL/SCI/TM48E

technical memorandum Daresbury Laboratory

DL/SCI/TM48E

SOFT X-RAY BEAMLINE FOR SURFACE EXAFS STUDIES IN THE ENERGY RANGE
60 < hr < 11100 eV AT THE DARESBURY SRS

by

A.A. MACDOWELL, D. NORMAN and J.B. WEST, Daresbury Laboratory.

APRIL, 1986

Science & Engineering Research Council

Daresbury Laboratory

Soft x-ray beamline for surface EXAFS studies in the energy range 60 < hν < 11100 eV at the Daresbury SRS

A.A. MacDowell, D. Norman and J.B. West,

SERC Daresbury Laboratory, Daresbury, Warrington WA4 4AD, England.

The characteristics of the beamline used for surface EXAFS (Extended X-ray Absorption Fine Structure) studies at the Daresbury Synchrotron Radiation Source are described. Monochromatic photons are available in the photon energy range 60 < hν < 11100 eV. This has been achieved using a monochromator with a combination of crystal and grating optics. The radiation is focused through the monochromator by a toroidal premirror at 0.5° grazing angle. Three pairs of crystals and a plane grating with focusing mirror are available which can be interchanged under UHV. The plane grating/mirror monochromator has two ranges of zero-order angles 6.4° and 2°, giving photon energy ranges of 60 - 550 eV and 600 - 2000 eV respectively with a 1200 ℓ mm^{-1} grating. The crystals in use are InSb(111), Ge(111) and Ge(220) having photon energy ranges of 1745 - 7360 eV, 2000 - 8430 eV and 3260 - 11100 eV. The performance of the gratings and crystals in respect of intensity, resolution, scattered light and higher orders is discussed and some representative results from the beamline are given. Detailed consideration has been given to thermal effects on the crystal and grating optics. The grating can be exposed to a maximum power density of 9 W cm^{-2} and has so far performed adequately. The crystals, which can see power densities of up to 150 W cm^{-2} have survived, but exit beam movement and energy scale shifts are observed. Efforts to reduce these beam movement effects have been successful inasmuch as the instrument is useable. InSb crystals suffered some radiation damage. Beryl and Quartz crystals have been tried but did not survive. Recommendations for the elimination of these beam heating effects are given, along with future improvements to reduce beam size at the sample for the grating/mirror part of the instrument.

SCIENCE AND ENGINEERING RESEARCH COUNCIL

DARESBURY LABORATORY

INTRODUCTION

The surface EXAFS (SEXAFS) technique[1] offers a powerful way of determining the atomic arrangement of solid surfaces. The potential of such experiments has been limited by the available technology and only within the last few years - since the more reliable high brilliance storage ring light sources became available - has there been a push towards standardisation of the technique.

SEXAFS experiments require a tunable monochromatic photon source. The output from bending magnets on storage rings is a broad continuum and thus a scanning monochromator is necessary to select the required wavelength. Ideally the monochromator should scan an energy range that covers as many elemental inner shell absorption edges as possible. Such an instrument would of course allow the greatest flexibility in the kind of experiment to be carried out. Other design constraints imposed by SEXAFS are the UHV nature of the experiment and the usual requirements for a small intense photon beam size at the sample.

With these requirements in mind we have built a windowless beamline for SEXAFS studies using radiation from dipole 6 on the 2 GeV Daresbury Synchrotron Radiation Source (SRS). This beamline is the subject of this paper.

I. DESIGN OBJECTIVES AND OPTICAL LAYOUT

The objective was to design a UHV-compatible (< 10^{-9} Torr) beamline which could supply to the sample (i) monochromatic radiation in the 0.1-10 keV range with a resolving power of ~ 500-2000; (ii) provide a high

intensity beam of small size ($\lesssim$ 5 mm^2) at the sample; and (iii) have a spatially fixed beam behind the monochromator.

These design objectives are similar to those of the JUMBO beamline[2] at Stanford. The main novel feature of our beamline is the very large (0.1-10 keV) energy range which has been achieved using a monochromator having in situ interchangeable crystal and grating optics. The crystal optics cover the higher energy range whereas the grating optics cover the lower energy range. The use of focusing optics provides the small spot size at the sample. The requirements of a spatially fixed exit beam after the monochromator needs the crystal optic part of the monochromator to be the double crystal +1, -1 configuration with the standard two rotations and one translation motion of the two crystals.

With these considerations in mind the beam line concept shown in Fig.1 was chosen. Figure 1(a) shows the optical arrangement for the beamline when used in the high energy double crystal mode. The radiation is collected by the toroidal mirror and focused through the double crystal monochromator onto the sample. The single toroidal mirror provides focusing in both the vertical and horizontal planes. The Bragg angular range is 13°-72°. This is essentially the same layout as used at Stanford[2].

Figure 1(b) shows the optical layout when used in the low energy grating mode. The radius of curvature of the toroid in the vertical plane is increased to provide parallel radiation onto the plane grating. This reduces focal shift when the monochromator is scanned. The dispersed monochromatic radiation is then focused by the spherical mirror onto the exit slit. The grating/mirror combination is based on the Miyake principle[3], and two ranges are available with zero-order angles of 2° and

6.4°. The choice of angles was based on Refs. 3, 4 and 5. The basic parameters for the grating/mirror monochromator are given in Table I for a 600 ℓ mm^{-1} and a 1200 ℓ mm^{-1} grating, although this paper reports only the results for a 1200 ℓ mm^{-1} ruling density. Focusing in the horizontal plane is provided by the toroidal premirror with the radiation focused through the monochromator onto the sample. In the vertical plane the radiation diverges from the exit slit. Both divergence and exit slit-sample distance should be small to reduce beam size in the vertical plane at the sample. The vertical displacement of beam is 20 mm for both the crystal and grating mode of the monochromator. The entire beamline is windowless.

II. FOCUSING OPTICS - THE TOROIDAL PREMIRROR

The high energy cut off is limited by this mirror and to achieve a cut off of ~ 10 keV a grazing angle of 0.5° is used with a gold reflecting surface[6]. The mirror is a fused quartz cylinder, 8 cm thick, 12.5 cm wide and 75 cm long[7]. This cylinder is bent to a toroidal shape using the concepts of Howell and Horowitz[8], and the results of setting up this mirror system have been reported previously[9]. Due to the relatively large size of the electron beam at dipole 6 of the SRS (6 mm horizontal × 1.2 mm vertical f.w.h.m.[10]), some demagnification is needed, and the mirror demagnifies the source 2:1 at the sample. The mirror is 11 m from the source point and can accept up to 5 mrad (horizontal) × 0.6 mrad (vertical) of synchrotron radiation. The focusing conditions[8] require the major and minor radii to be 840 m and 6.4 cm respectively when focusing in both horizontal and vertical planes onto the sample.

The bending of the cylindrical mirror is achieved using the mechanism shown in Fig.2. The mirror is supported on its base at its two ends. This

support is substantial and extends to the large vacuum flange on which the mirror is effectively mounted. At a distance of 9 cm from the ends of the mirror, four aluminium pads sit on its top outer rim. These are connected to a central rod which, when pulled in a downwards direction exerts the necessary opposing couples to bend the mirror into a toroidal shape. This central pulling rod connects through the vacuum via bellows and has its end threaded with a 2.25 mm pitch. This central rod is pulled down by means of a differential screw system consisting of a special nut of inner thread pitch 2.25 mm and an outer counter thread of pitch 2.50 mm. Thus one full turn of this nut by means of the manual wheel pulls the rod down by 0.25 mm. Most of this movement bends the out-rigger arms from the central rod but some moves the aluminium pads downwards the required 19 μm. The maximum required sagitta of the mirror is 84 μm. This can be monitored by means of a dial gauge mounted on the top outer rim in the middle. Movement is transferred outside the vacuum via bellows. The flexing of the mechanism as a whole is monitored by means of two similar dial gauges which are in contact with the lower surface of the mirror at its ends. We find that the whole mirror lowers by 1 mm as the mirror is bent to the minimum major radius of 840 m. This is due to flexing of the main end supporting structures. To compensate for this the whole assembly is raised by 1 mm on its supports.

The thermal load on the mirror was given consideration. For a gold reflecting surface incident to the synchrotron radiation at a grazing angle of 0.5° it was estimated that ~ 10% of the thermal power of the beam would be absorbed by the mirror. The maximum power from the SRS is 12 W $mrad^{-1}$ at 300 mA, 2 GeV. This results in a maximum absorbed power density of ~ 0.02 W cm^{-2} on the mirror surface and a total maximum absorbed power of ~ 6 W. This power loading is low[11] and it was not expected that the mirror

would have to be forcibly cooled. In practice we have found no evidence of thermal effects on the focusing properties of the mirror. If the white synchrotron radiation were allowed to hit the end of the mirror which directly faces the beam, however, considerable heat loads would be expected. The end of the mirror was protected by an uncooled oxygen free copper plate with a slot shaped to accept the useful synchrotron radiation. It was not considered necessary to cool this plate because although it gets hot (~ 200°C), outgassing is relatively low from the pure oxygen-free copper. Also the premirror section does not need to be truly UHV as it is well differentially pumped from the storage ring at one end and the experiment at the other - both requiring UHV (< 10^{-10} Torr). The main vacuum requirement for the premirror section is to be hydrocarbon free to reduce contamination on the mirror.

The same arguments apply to the uncooled beam defining apertures in front of the premirror 10 m from the source point. The horizontal aperture is adjustable by means of two independent side jaws. The vertical aperture selector consists of a series of preset slits on a manual linear motion drive that allows vertical apertures of 0.05, 0.1, 0.2, 0.3, 0.4, 0.5 and 0.6 mrad to be selected. A pneumatically operated water-cooled copper mask positioned upstream of the apertures can be used to mask off the beamline optics.

III. THE MONOCHROMATOR

This is shown schematically in Fig.3. The double crystal monochromator section consists of three pairs of crystals (Ge(111), InSb(111) and Ge(220)) of crystal dimensions 25 × 25 × 3 mm. The crystals are front surface mounted in replaceable crystal holders, and can be translated as a

pair into the beam by means of a manual linear drive. The crystals require two rotations and one translation to achieve constant vertical deviation. These motions are transferred into the vacuum chamber by means of three independent linear drives. The two rotations are then achieved by means of internal sine bars. The upper crystal receives the white beam and this crystal simply rotates about its front surface. Monochromatic radiation is Bragg reflected to the lower crystal which has to translate and rotate. The lower crystals are mounted on a linear translation carriage which runs on two precision-round bars that are parallel to the horizontal optical axis. The optical flat for the small wheel bearing at the end of the sine bar for the lower crystal rotation is arranged to be parallel to the horizontal optical axis. The Bragg angular range is 13°-72°.

The lever arms of the sine bars were arranged to be approximately parallel to the horizontal optical axis at the mid Bragg angle of the instrument (42.5°). The lever arm length was chosen to be 208 mm such that a 1 μm linear motion rotates the crystals by ~ 1 arc second throughout the angular range. Optical interference encoders[12] with a resolution of 0.1 μm are attached to the lead screws of the linear motion drives. Stepper motors, powered via sine-cosine drives to ensure smooth accurate running, are used to operate the linear motion drives. Positioning of the linear motion drives to ± 0.3 μm is easily accomplished. The total motion of the sine bar linear motion drive is 200 mm. To ensure a true linear motion of the lead screw over this long range it is guided internally by means of a linear bearing assembly. The vertical displacement of the outgoing monochromatic beam is 20 mm, requiring a total horizontal translation of the lower crystal carriage of 70 mm.

The grating/mirror section of the monochromator consists of a fused

silica 1200 ℓ mm^{-1} platinum-coated laminar grating[13] (25 × 25 × 8 mm) and a gold-coated 5 m radius spherical mirror in the Miyake configuration[3]. The grating/mirror combination can be translated into the beam using the same manual linear drive that translates the crystals. The grating is mounted on the same rotation assembly as the top crystals and its rotation is performed by the same motor/sine bar assembly. The mirror has to translate and rotate allowing for zero-order angles of 2° and 6.4°. To achieve this, the mirror is mounted on an entirely separate carriage that can be rotated and translated by another two independent linear drives. This carriage runs on the same two parallel reference bars as the lower crystals. The total translation required for the mirror is a distance of 200 mm. This is achieved using a similar linear drive with encoder as for the crystal motions. As the translational position requirements of the mirror are not critical to better than ~ 50 μm costs were reduced by using a linear drive of only 100 mm travel with an internal 1:2 cantilever mechanism to allow the necessary 200 mm total. The rotation of the mirror is accomplished using a similar sine bar assembly as for the lower crystal assembly. The exit slit of the monochromator is in the dispersion plane of the grating/mirror combination. It has two ranges - fine (5-500 μm) and coarse (0.5-6 mm). The fine range is used to determine the resolution from the grating monochromator. The coarse range simply allows the slits to be fully opened more rapidly for use in the crystal mode.

The entire monochromator is made from stainless steel, with phosphor bronze being used in combination with stainless steel where friction is inevitable in the unlubricated uhv environment. High quality precision stainless steel bearings are used for all rotations. The entire instrument fits into a cylindrical vessel about 750 mm in diameter × 450 mm high pumped by a 400 ℓ s^{-1} ion pump and a 1000 ℓ s^{-1} titanium sublimation pump.

All the five drives are under the control of a PDP-11 computer interfaced to CAMAC hardware. The crystal holders come within a distance of ~ 3 mm on their closest approach (45° Bragg angle). Because the crystals are independently driven, computer error, an encoder error or motor fault could result in the crystals colliding, with consequent damage. To prevent this, a dummy pair of crystals slightly larger than the real ones is installed on the crystal rotation axes. One dummy holder is electrically isolated such that when the two holders touch, a hardwired circuit stops all motors. The system can then be reset manuallly.

IV. MONOCHROMATOR OPERATION - DOUBLE CRYSTAL MODE

A total of 2 μm thickness of carbon, composed of one rack of ten self-supporting carbon filters[14] each of thickness 2000 Å, is inserted into the white beam before the toroidal premirror to remove the ultra violet component of synchrotron radiation which would otherwise specularly reflect from the crystal surfaces and be transmitted by the monochbromator. This is considered in greater detail in section V.D. The premirror is bent to its fullest extent to focus radiation in both horizontal and vertical planes onto the sample. The apertures in front of the premirror are usually wide open and the entrance slit to the monochromator is simply used as an angular aperture to remove stray light around the edges of the beam. The focused spot size on the sample is 4 mm wide × 1 mm high f.w.h.m., this being the result of the 2:1 demagnification + aberrations of the source (6 mm × 1.2 mm f.w.h.m.).

The angle and position of the crystals is calculated from the simple trigonometry of the instrument. Owing mainly to thermal effects (see section V.E) rotation of both crystals by dead reckoning is not sufficiently accurate and the crystals then have to be fine tuned to transmit the required part of the rocking curve. This is achieved by monitoring the output x-ray inteneity and using this as a signal for a feedback loop.

The output beam monitoring section after the monochromator is shown schematically in Fig.4. It consists of two transmission photodiode detectors separated by a rack of beam defining apertures. The first photodiode (I_0') is made from 86% transmittance copper mesh. The drain current is measured directly with a picoammeter whose output is connected to a voltage-to-frequenoy converter and then to a CAMAC scaler. Currents in the range 10^{-11}–10^{-9} A are observed, depending on ring current, crystals and Bragg angle. Careful attention is paid to the shielding of these small currents. This first monitor sees the entire Bragg peak output from the monochromator. The beam can then be reduced in size to match the sample size using the apertures and the resulting transmitted flux of x-rays (incident on the sample) is then measured by the second photodiode (I_0) consisting of four different transmission photodiode materials, interchangeable in situ. These are 2.5 μm beryllium foil, 0.7 μm aluminium foil, 86% transmission copper mesh and 92% transmission tungsten mesh. The drain current is measured directly with a picoammeter. Generally above 2000 eV the 0.75 μm aluminium foil is used as this gives the largest signal. The 1745-2000 eV range (covered by the InSb(111) crystals) is monitored using the beryllium foil because aluminium EXAFS can interfere in this region. The foils/meshes can be rotated to face an ion gun for periodic cleaning if they become contaminated with an interfering element. Argon or oxygen are the cleaning gases used. Argon embeds itself in the monitor and produces an edge at 3206 eV so oxygen can be used to clean the monitor if the argon edge interferes with the scanning range. A rack of

calibration foils can be inserted in front of the I_0 monitor to check the energy scale of the monochromator.

Only the first monitor (I_0') is used to provide the signal for the feedback loop. This feedback loop is entirely under computer control. In operation the computer synchronously drives the three motors to encoder readings calculated from the simple trigonometry of the instrument. At the first point of the scan the calculated position of the crystals usually results in no output from the monochromator due to thermal effects on the first crystal (see section V.E). The top crystal is then rapidly rotated back and forth until a signal is obtained from the I_0' monitor. Rotation of the top crystal then proceeds more slowly as the crystal is rotated in small steps and the rocking curve mapped out. At each step the I_0' signal is monitored for 100 ms by the CAMAC scalers. The step size is scaled to the Darwin width of the rocking curve and is ~ 0.02 × Darwin width. The top of the rocking curve is established by moving three steps over the peak to prevent spurious noise from imitating the maximum of the rocking curve. The top crystal rotation encoder is then read, which when subtracted from the calculated encoder reading provides an initial offset (dependent on top crystal heat load) that can be used as the starting point to speed up the peak-search for the next point in the scan. If the user requires the maximum output from the monochromator, the crystal is rotated back three steps to the top of the rocking curve. If harmonic rejection is required the monochromator has to sit at a given percentage of peak height on the side of the rocking curve[15]. In this case the top crystal continues to be stepped until the monochromator output is equal to the required fraction of the peak height measured in the peak finding section. Because the harmonic rejection output is on the steep gradient of the rocking curve, the step

size used reduces as the correct output signal is approached. Step size at the final approach is ~ 0.005 × Darwin width.

Note that the I_0' photodiode mesh wires are at 45° to the horizontal (Fig.4). This is necessary because during a peak search there is a vertical displacement of the beam during the mapping out of the rocking curve. If the wires were horizontal the I_0' response would be step-like in nature as the beam is moved vertically over each wire. The use of two beam monitors (I_0' and I_0) has proved to be necessary due to this vertical beam movement during peak search. The first monitor (I_0') is required to "see" the entire rocking curve profile in order to provide the correct feedback signal to select the required part of the rocking curve to be transmitted. The second monitor (I_0) "sees" a convolution of the rocking curve with the angular acceptance of the aperture. Using this as the feedback signal does not give satisfactory results.

For the next photon energy in the scan the lower crystal is driven to the calculated position from the trigonometry of the instrument. Using the value learnt from the previous point the top crystal is rotated to an encoder reading that positions the output near the top of the rocking curve. Only the very top of the rocking curve is mapped out this time and then the monochromator is positioned where required on the rocking curve. Once the monochromator has learnt the offset value from the first point, the time for the monochromator to move from one photon energy to the next is ~ 2-3 s. The top of the rocking curve is determined to better than 0.1%, this being the variation in output from point to point in the scan.

This feedback system described is similar to the one employed to drive the JUMBO monochromator[16]. The main difference is that our monochromator

remains entirely under computer control whereas in the Stanford instrument, the peak is established using an analogue differentiating circuit. Note also that our monochromator is stationary during the data collection time. The flux output is therefore constant during this time, whereas other feedback techniques employed on double crystal monochromators result in a monochromator output that is constantly oscillating (see for example ref.35).

V. PERFORMANCE - DOUBLE CRYSTAL MODE

A. Mechanics

The positions of the internal sine bar mechanisms of the monochromator are measured outside the vacuum using the optical linear encoders. The ability of these to represent faithfully the rotations of the crystals is of vital importance to the operation of the monochromator. To check the repeatability of the rotation drives, rocking curve profiles were plotted against encoder reading by keeping one crystal stationary and rotating the other. The crystal that was rotated was driven from either direction several times. Errors in the rotation mechanics of the moving crystal would appear as a displacement of the rocking curve relative to encoder position. Although sine bars are in principle backlash free we observed an apparent backlash of ~ 2 arc seconds. This can be explained by small radial clearances in the ball bearings. For driving in one direction it was found that the absolute repeatability of the rotation has a standard deviation of ± 1.0 arc seconds. Both top and bottom rotation mechanisms behaved identically. In view of the rocking curve widths of the crystals used ($\gtrsim$ 30 arc seconds) these driving accuracies are more than adequate.

The energy calibration of the instrument is obtained from simple trigonometry. Using the thin foils in the exit beam monitoring section the

calibration accuracy over its entire angular range is found to be well within the experimental error of determining where the elemental edge is. No evidence of calibration errors due to mechanical inaccuracy has been found.

B. Crystals, energy range and output

Three crystal pairs are in use. The 2d spacings and energy ranges are InSb(111) (2d = 7.4806 Å, 1745-7360 eV), Ge(111) (2d = 6.532 Å, 2000-8430 eV) and Ge(220) (2d = 4.00 Å, 3260-11100 eV). The measured outputs from the crystals are shown in Figs.5, 6 and 7 with the SRS operating at 2 GeV. The absolute number of photons per second per 100 mA was determined using the 0.75 μm oxidised aluminium I_0 monitor and the photoemission yields of Henke et al.[17]. Two photoemitting surfaces were assumed and the photon attenuation by the foil was taken into account using the cross-sections of Viegele[18].

Figure 5 shows the transmission function of the InSb(111) crystals. The gold M edges from the premirror and the indium and antimony edges are identified. Several spurious crystal glitches are present. These are a problem and are further discussed in Section V.D. We have observed short term changes of our InSb(111) crystals. In the low energy region the new crystals produced four glitches at 1848, 2029, 2139 and 2144 eV. After 30 A h of beam where the first crystal temperature reached ~ 200°C there were only three glitches at 1850, 2035 and 2110 eV. It seems as if the crystal suffered annealing. The crystals remained stable then for over one year of use (~ 2000 hours exposure) until continued use at large Bragg angles with high currents (300 mA, 2 GeV) resulted in the surface melting of the first crystal. The bulk melting point of InSb (535°C) gives an indication of the surface temperature reached for maximum power input

(50 watts, ~ 150 watts/cm^2). The InSb(111) crystals now have to be used with a smaller aperture to reduce power loading.

The Ge(111) transmission function (Fig.6) shows the gold M edges from the premirror. Two contaminants, phosphorus from an experiment and argon from the ion cleaning gun are readily identified. Numerous cryetal glitches are also present.

The Ge(220) crystals transmission function (Fig.7) shows several glitches similar to the other crystals. The high energy cut off is at 11.1 keV due to the germanium K edge. It is interesting to note that 11 keV photons are still reflected by a gold-coated mirror at 0.5° grazing angle. The low energy cut off is characterised by a rapid reduction in intensity. The Bragg angles used in this region are around 70° so the thermal power density on the first crystal is substantial (see Section V.E). For Ge(220) with its relatively narrow rocking curve the displacement of the heated crystal's transmission on the DuMond diagram (ref. 19 and Appendix 1) is such that it does not overlap greatly with that of the second unheated crystal. The result is a reduction in the transmitted x-ray flux.

Other crystals that have been tried have been Si(111) (2d = 6.271 Å), beryl ($10\bar{1}0$) (2d = 15.954 Å) and α-quartz ($10\bar{1}0$) (2d = 8.512 Å). The first crystal in the pair of beryl and quartz crystals broke in the intense white radiation. The Si(111) crystals performed adequately but because their energy range is similar to Ge(111), and transmitted flux approximately 2-3 times lower, the Si(111) crystals are generally not used. The reason for the reduced light throughput by the Si(111) crystals is their narrower rocking curve. This has little effect on resolution which is dominated by

the convergence of the radiation through the monochromator (see next section).

C. Rocking curves and energy resolution

Rocking curves are easy to measure with this instrument using the independent rotations of the two crystals. Double crystal rocking curve half widths for the three crystals InSb(111), Ge(111) and Ge(220) were measured under low thermal load (SRS operating at 1.8 GeV, 100 mA) and are shown in Fig.8 as the solid lines. The Ge(111) rocking curve is comparable with that obtained at Stanford[16]. The InSb(111) rocking curve compares similarly with that obtained at the Photon Factory[20] which is better than that obtained at Stanford[16]. The dashed lines of Fig.8 are measured rocking curves under more normal operating conditions (2.0 GeV, 250 mA). The rocking curves are broader due to the gradient change of the heated first crystal's output on the DuMond diagram (see Appendix).

By differentiating Bragg's Law the energy resolution (ΔE) of the crystal monochromator is given as

$$\Delta E = \frac{2d\ E^2\ \Delta\theta\ \cos\theta}{12398}\ \text{eV} \qquad (2)$$

where θ is the Bragg angle, 2d is the crystal spacing and E is the photon energy (eV). The angular half width term Δθ can be approximated by summing quadratically the various half width angular contributions from the beamline components

$$\Delta\theta = (\Delta\theta_{SR}^{\ 2} + \Delta\theta_{S}^{\ 2} + \Delta\theta_{C}^{\ 2})^{1/2}$$

where $\Delta\theta_{SR}$ is the convergence angle through the monochromator (this being twice the vertical angular divergence of the radiation given by Ref.21), $\Delta\theta_S$ is the angular source height as seen by the premirror (22 arc. sec.) and $\Delta\theta_C$ is taken to be the double crystal rocking curve width which as discussed in the appendix represents the upper limit for the angular contribution from the crystals.

Calculated plots of resolution for the three crystal pairs are shown in Fig.9. Here three different angular combinations are shown. The full line denoted by C represents the resolution when considering only the rocking curve width and represents the ultimate resolution attainable. The other full line (denoted by C + S + SR) represents the resolutions for the usual beamline conditions taking into account the crystal rocking curve, source height and divergence of the radiation. As can be seen the resolution for the low energy ranges of the crystals maintains a $E/\Delta E$ value > 1500. For the high energy end the resolution degrades to $E/\Delta E \sim 400$ because the angular convergence of the radiation through the monochromator dominates the $\Delta\theta$ expression.

The resolution can be improved at the expense of light flux at the sample. Two methods are available - collimation of the beam using the vertical apertures before the premirror or unbending the mirror to send parallel radiation onto the crystals. Both have the effect of reducing $\Delta\theta_C$. The dashed lines of Fig.9 show the calculated resolutions for $\Delta\theta_C = 0$. For these plots, only the crystal rocking curve and source height are considered. As can be seen the source height becomes important only for high energies. An example of unbending the premirror is given in Fig.10, which shows the transmission EXAFS of a 10 μm titanium foil with the premirror bent and unbent, using the Ge(111) crystals. Total photon

flux has however reduced by about a factor of 4 due to bandpass reduction and the radiation is no longer focused in the vertical plane. The calculated resolution improvement is from 9.0 to 2.4 eV.

Knowing the bandpass it is possible to calculate the efficiency of the crystal monochromator. For InSb(111) and Ge(111) at 3 keV the efficiencies are 5% and 5.7%, respectively. For Ge(220) at 5 keV the efficiency is 9.3%.

D. Stray light, crystal glitches, normalisation

It is necessary to remove the UV/visible component of the synchrotron radiation which would otherwise specularly reflect from the crystal surfaces and be transmitted by the monochromator. The following methods are employed at Daresbury to achieve this:

(a) In normal use a rack of 10 × 2000 Å carbon filters (total thickness 2 μm) is inserted into the beam before the premirror. They effectively eliminate $h\nu < 100$ eV. When using high energy photons ($\gtrsim$ 6 KeV), the low Bragg angles favour specular reflection. A 250 μm beryllium filter (cut off ~ 2.5 keV) can replace the carbon filters in this case. The filters are positioned in front of the premirror to reduce the total light flux falling on the mirror. This might be expected to reduce the carbon contamination rate.

(b) The crystals are cut with their surface face offset by 0.5° from the Bragg planes. The specular reflected light thus propagates along a different direction from the monochromatic x-rays.

(c) The manufacture of the InSb(111) crystals included etching which resulted in a substantial surface pitting of the crystal. This has no

effect on the Bragg reflected x-rays but the specular radiation is scattered to such an extent that very little is transmitted by the monochromator even when the filters are removed.

We do not observe a problem with scattered light. A crude attempt to measure the intensity of specularly reflected radiation with the carbon filters in indicated a contribution of $\lesssim$ 0.1% of that of the monochromatic x-rays. This specular light would, however, not be following the direction of the x-rays and would not even be able to pass through the monochromator exit slit.

Crystal glitches have been mentioned in section V.B when the monochromator output was discussed. We find that crystal glitches are difficult to normalise out of total yield SEXAFS data where the sample signal is only ~ 1% of the total. For bulk total yield EXAFS we find the stronger signal allows normalisation.

Crystal glitches are the result of multiple Bragg reflections between the main reflecting plane and higher order planes. They can arise from higher order planes within a single crystal or from the reflections of high order planes in both crystals. Misorientating the crystals with respect to the x-rays and each other but keeping the main reflecting planes parallel (i.e. rotate the crystals about their poles) are the usual ways of eliminating glitches. Our attempts to follow this approach have not been very successful. Two techniques have been tried to reduce the glitch content:

(i) The crystals are orthogonal to each other with respect to their original position in the boule from which they were cut. This ought to reduce

the number of spurious reflections between higher order planes of the two crystals.

(ii) The top crystals can be rotated in situ by ± 12° about their poles using a wobble stick assembly. The effect on glitches was very limited. For some glitches there was no effect, for others only a very slight 10-20% change in intensity. The remaining technique of removing the crystals and randomly reorientating them has yet to be tried. The UHV nature of the instrument does not lend itself to this type of experiment.

Another effect that might have been expected arises from the relatively large convergence angle of the x-rays through the monochromator (up to 1.1 mrad) and the narrow rocking curves that these high-order glitch planes should have. It might be expected that the crystal glitch may be spatially distributed in the outgoing monochromatic beam. This we find to be so for some glitches, such that by selecting out different sections of the output beam using the aperture mask in the beam monitoring section (Fig.4), monochromatic radiation with a high or low glitch content can be chosen. This has not proved very useful so far due to output beam movement effects caused by first crystal heating (see next section).

Finally we note that the gold M edges present in the transmission function of the crystals do appear to normalise out from SEXAFS data taken to date.

E. Beam movement and thermal effects

A major problem in operation of the double crystal monochromator has been the thermal loading on the first crystal, which is exposed to the partially focused, white synchrotron radiation beam. Heat loads of up to 50 W with a power density of ~ 150 W cm^{-2} are possible with the SRS running

at 2 GeV, 300 mA. This can result in a differential temperature of over 200°C between the two crystals. The heating of one crystal results in an increase in the 2d spacing and a consequent shift in the energy scale and a vertical deflection of the monochromatic beam. The energy scale also becomes non-linear.

The reason for the vertical deflection of the beam can be seen from Fig.11 which shows that the first (heated) crystal has to be rotated by an angle β from the true parallel configuration before x-rays are passed by the system. The change in energy scale arises from the change from θ_0 to $\theta_0 + 2\beta$ in the Bragg angle of reflection from the lower (cold) crystal. A complete analysis of the angles, energy scale shifts and heat densities associated with +1, -1 double crystal monochromators is given by Rowen et al[23].

These effects are dependent on the thermal density of the white beam on the first crystal. Thus the beam moves and the energy scale shifts during both the decay of the beam and during a scan where the Bragg angle changes with consequent change in power density on the first crystal. The distance between the crystals and the sample has been kept as short as possible (1.5 m) thus reducing the lever arm length. Beam movement cold+hot for the InSb(111) crystals at 70° Bragg angle is ~ 8 mm for 2 GeV, 250 mA. For the germanium crystals the situation is a little better due to the higher thermal conductivity of germanium compared to InSb.

The experimenters find the worst problem is beam movement during the scan, i.e. actually recording a spectrum. The shift in energy scale and linearity of the scale can in principle be manipulated on a computer at a later date if it is considered necessary. We have adopted several means in an attempt to alleviate the problem:

(i) The use of copper radiation cooling fins pressed onto the rear of the crystal and thermally coupled by means of a gallium metal interface[24] reduces the crystal temperature somewhat. The ability of gallium to etch into other materials has been described by Hunter and Williams[25]. Our crystals are 3 mm thick and we have observed no problems in the year the gallium has been in use.

(ii) The use of the apertures in the I_0 monitor section allows the beam to move over them vertically while still maintaining a virtually constant beam position at the sample. The photons passed by the aperture are monitored by the I_0 monitor, thus allowing the variation in x-ray intensity during a scan due to beam movement to be normalised out.

(iii) By rocking the top crystal off the Bragg peak significant vertical displacements of the exit beam are possible due to the large rocking curve widths at large Bragg angles. Higher order suppression (obtained by rocking off the peak) is required in this region. Also the vertical deflection of the exit beam by first crystal heating is greatest at the larger Bragg angles. Thus, the vertical deflection of the exit beam due to heating can be counterbalanced by rocking off the Bragg peak for higher harmonic rejection.

Generally, however, the heating effect remains a problem and ways of cooling the first crystals are under consideration.

VI. SEXAFS SPECTRA USING THE DOUBLE CRYSTAL MODE

The instrument is in routine use for surface EXAFS measurements, and its capability is illustrated by Fig.12 which shows the spectrum[26] from a half-monolayer c(2 × 2) coverage of S on Ni(110). This spectrum, measured by monitoring the S KLL Auger yield, was taken in one single sweep with about 30 min. data collection time, and indicates the good signal-to-noise ratio attainable.

The usefulness of the wide energy range of this instrument is demonstrated in fig.13, which shows the Fourier transform of EXAFS spectra from a cleaved crystal of gallium sulphide[27], measured at the S K-edge (~ 2472 eV) and the Ga K-edge (~ 10367 eV). These spectra were measured using the Ge(111) and Ge(220) monochromator crystals respectively. The strong polarisation dependence is evident in this anisotropic crystal structure.

The lowest energy absorption edge presently attainable with this double crystal instrument is the Si K-edge at ~ 1840 eV. Figure 14 depicts a SEXAFS spectrum for the photon-stimulated desorption of H^+ ions from water adsorbed on a Si(100) surface[28].

VII. MONOCHROMATOR OPERATION - GRATING MODE

The mechanics of the grating/mirror assembly has been described in Section III. The grating part of the monochromator is unable to accept a large aperture and maintain reasonable resolution at the same time. This is a characteristic of the Miyake type monochromator and is due to the aberrations associated with the use of spherical optics with high demagnifications in grazing incidence.

To convert from crystal to grating mode it is first necessary to reduce the aperture accepted by the beamline. Typical apertures are 0.1 (V) × 0.5 (H) mrad for the 6.4° range and 0.05(V) × 0.5 (H) mrad for the 2° range. The requirement to reduce the aperture as the first stage of the conversion is primarily for safety as it is possible, if the correct procedures are not followed, to irradiate the fused silica grating with the full intensity of the focused white radiation at near-normal incidence. Although we have not yet tried this, our experience with fused silica under power densities of 40 W cm^{-2} suggests the grating would be damaged[24]. However by exposing the grating only at grazing incidence to apertured radiation we observe no appreciable change after 20 A h usage. The maximum radiation density on the grating is calculated to be ~ 9 W cm^{-2} with total power of 2.1 W. The coating of the grating was chosen to be platinum rather than gold because the latter has been observed to surface melt under high thermal loads of synchrotron radiation when on a poor thermally conducting substrate like fused quartz[29]. Platinum, with its higher melting point, does not suffer to such an extent.

The premirror is partially unbent (major radius = 2500 m) to provide parallel radiation for the monochromator. The filters in front of the premirror are removed. The entrance slit of the monochromator is set to the same value as the vertical aperture accepted by the beamline. The slit serves only as an angular aperture to remove scattered radiation from around the main central beam. The crystals are driven to the 70° Bragg angle position. This positions the lower crystal carriage at the far right-hand side of the monochromator (Fig.3), allowing the required range of movement necessary for the focusing mirror carriage. The top crystal rotation (on which the grating is also mounted) is rotated to the required angle. The grating/mirror assembly can then be translated into the beam

using the manual linear drive. The spherical mirror carriage is translated and rotated to the correct position depending on whether the 2° or 6.4° range is required. The exit slits are closed down to the required resolution setting. Scanning is achieved simply by rotating the grating.

The conversion of the beamline from crystal mode to grating mode requires numerous precision movements in vacuum. We find the beamline can be changed from one operational mode to the other in s repeatabie manner. With experience the conversion time is < 10 min.

VIII. PERFORMANCE - GRATING MODE

The output of the monochromator using the 1200 ℓ mm^{-1} grating for the two ranges is shown in Figs.15 and 16. The absolute number of photons was determined using the oxidised 0.75 μm thick aluminium I_0 monitor, in the same manner as used for the crystal transmission functions. The scattered light content was estimated by extending the zero-order tail. Higher order content has not been measured.

Figure 15 shows the output for the 6.4° range which extends from 60-550 eV. The large dip at the carbon K-edge is caused by contamination on the premirror which has been installed for over four years. Scattered light is a problem for this range due to the grazing angles. Inserting the 2000 Å carbon filter in front of the premirror reduces the scattered light by a factor of 3. The transmission function of carbon[18] results in a substantial reduction in light in the ~ 60 - 150 eV and 280 - 400 eV regions. For the regions ~ 150 - 270 eV and above ~ 400 eV the monochromator throughput is only slightly reduced by the 2000 Å carbon filter.

The source size limited resolution measured at zero order was 0.07 Å f.w.h.m. which is less than the value (0.1 Å) calculated using a

source height of 1.2 mm. We can only assume the source was smaller in height than calculated[10]. The use of spherical optics at grazing incidence gives rise to substantial aberrations. The two focusing optics (the toroidal premirror and the 5 m radius spherical mirror) both focus in the vertical, dispersion plane. Both are deflecting the beam vertically and in this optical arrangement coma is self-corrected. Good focusing properties were expected and realised.

The radiation diverges in the vertical plane from the exit slits to the sample. With the 0.1 mrad entrance aperture the resultant divergence from the exit slits is 3.8 mrad. The exit slit to sample distance is 925 mm resulting in a vertical beam height at the sample of ~ 3.5 mm. As originally conceived ths exit slit-sample distance was to be about half its current value. Experience with the crystal monochromator section required the development of the beam monitoring system such that the sample had to be moved further away from the exit slits. Horizontal size of the beam at the sample is about the same as that for the crystal optics because the premirror is focusing in the horizontal for both operational modes. The reduced horizontal aperture taken by the grating allows for some reduction in horizontal width at the sample to ~ 3 mm f.w.h.m.

The copper or tungsten I_0 meshes are usually used for monitoring the beam from the grating. Using a clean copper mesh we were unable to observe any oxygen K-edge absorbtion at 520 eV from the optics which although gold- or platinum-coated are all fabricated from fused silica. The calculated efficiency at 400 eV is 0.2% showing the well-known inefficiency of grazing incidence optics compared to the high crystal optic efficiencies (section V.C).

Figure 16 shows the output from the 1200 ℓ mm^{-1} grating with the 2° zero-order angle. A smooth output curve is measured extending from 600-2000 eV and peaking at 1500 eV. Scattered light can be substantially reduced using the 2000 Å or 2 μm carbon or the 1.5 μm aluminium filters.

The aberrations of the spherical optics for the 2° grazing range are more severe than for the 6.4° range. Coma is the dominant aberration and in order to obtain the greatest benefit of the coma-corrected two mirror system the major radius of the premirror has to be changed to ~ 1500 m (radius = 2500 m for 6.4° range) to allow the coma of the premirror to be a better match to that of the 5 m radius spherical mirror. The best resolution achieved was 0.04 Å at zero order (0.03 Å is the theoretical source size limit).

The divergence in the vertical plane from the exit slits is particularly large for the 2° range due to the short mirror-slit distance of 88 mm. With an aperture of 0.05 mrad (vertical) × 0.5 mrad (horizontal) the beam size at the sample is 5.5 mm (V) × 3 mm (H). The efficiency of the monochromator is estimated to be 0.45% at 1500 eV.

As an example of the performance of the grating part of the monochromator, Fig.17, illustrates the resolution attainable from the instrument as it is scanned through the $2p_{1/2,3/2}$ edges of calcium present in an aluminium alloy sample. Note that the peaks are chemically shifted from the clean Ca positions, which are visible as shoulders at lower binding energies.

By comparison with other grating monochromators the output from this instrument is rather low. With new optics the output from the Grasshopper

monochromator at Stanford is approximately an order of magnitude higher[30] and the high energy TGM at DESSY[31] with its high aperture acceptance is about three orders higher. This is of course consistent with the small aperture that the Miyake design can accept when the aim is to produce a compact instrument such that the exit arm is short and high demagnifications are used. The resolution of the instrument is comparable to other instruments. The higher order suppression, although untried, is expected to be good. The problem of normalisation of flux has not been addressed, and the scattered light contribution has not been accurately measured: these are key factors for successful SEXAFS measurements in this spectral region[32].

IX. OVERALL PERFORMANCE AND FUTURE IMPROVEMENTS

It is interesting to compare the original design aims to those realised in practice. A wide photon energy range has been achieved, with photons observed between 0.06 and 11.1 keV.

In the crystal mode using Ge(111), InSb(111) and Ge(220) the resolution is reasonable for the lower energy ranges (large Bragg angles). Resolution does degrade at the smaller Bragg angles due to the relatively larger angular contribution from the beam convergence through the monochromator. However, using collimation, resolution can readily be improved at the expense of intensity. The flux throughout is comparable with other instruments.

The high thermal load on the first crystal has considerably restricted the types of crystal which can be used. Thus the difficult region ~ 700-1700 eV has not been covered using crystals of large 2d spacing (beryl and quartz broke in the beam). In this region we must use the 2°

high energy grating but the resolution attainable is approximately one order of magnitude worse than that from large 2d crystals (compare beryl $(10\bar{1}0)$ at 1000 eV, $\Delta E \simeq 0.6$ eV[16] and 2° grating range $\Delta\lambda = 0.04$ Å (at 1000 eV $\Delta E \simeq 3.3$ eV)). The throughput is also lower. To improve the situation in the 700-1700 eV range it is necessary to improve the grating and/or the crystal monochromator sections of the monochromator. There is not a great deal of flexibility in the grating section for improved performance. Increasing the line density on the grating improves resolution at the expense of spectral range due to the horizon cut off. It is, however, proposed to reduce the source size at the SRS by the installation of a new higher brightness lattice. The predicted source size is 2.4 mm (H) × 0.3 mm (V)[10] (compared with current size of 6 mm (H) × 1.2 mm (V)). This would improve resolution from the grating (in the absence of aberrations) by a factor of ~ 3-4 making the 2° range of the grating significantly more useful. To improve the crystal section for this energy range we propose to use a matched multilayer with a 2d spacing a multiple of the 2d spacing of KAP (100) or beryl $(10\bar{1}0)$. Thus a multilayer of 2d = 31.9 Å could be used in second order with a beryl crystal in first order. The multilayer would act as the first crystal and see the white beam. The use of higher orders from the multilayer allows one to use larger 2d spacings which are easier to fabricate than small values.

The original aim of constant deviation has proved difficult to attain due to heating of the first crystal. As noted in section V.E, we are considering cooling the first crystal by supplying water pipes to a copper block mounted on the rear of the crystal. Gallium will be used as the thermal interface between the crystal and the copper block. On another recently installed double crystal monochromator we have found that such a cooling system works well for crystals of reasonable thermal conductivity.

The size of the beam on the sample when the grating is in use is rather larger than was originally intended due to the development of the beam monitoring section and consequent increase in the exit slit-to-sample distance. To reduce the beam size at the sample we propose to move the exit slits to the current position of the apertures now used in the beam monitoring section. The slits will be adjustable in height and will have independent side adjustment apertures. These slits will be used both to define the resolution of the grating monochromator and also to aperture down the monochromatic radiation when used in the double crystal mode. The slits are to be adjustable in height to cope with the small vertical beam movements from the double crystal monochromator that will result even though the first crystal is water-cooled as some increase in the 2d spacing of the first crystal is inevitable. Also rocking off the peak results in a vertical displacement of the beam. Both of these displacements will be small at the sample (< 1 mm) so height adjustment of the exit slit allows for fine tuning of the required aperture. The effect of moving the exit slits results in a different grating slit distance and the use of one concave focusing mirror for two ranges is not possible with these new dimensions. A separate mirror is required for each range of the grating/mirror monochromator section in a similar manner to the instrument described by Howells[5]. Unlike the instrument described by him we do not propose to use off axis paraboloid mirrors - ray tracing indicates that spherical mirrors will be adequate, and these can be made with the required precision in figuring. We also propose to increase the number of ranges from two to three with zero-order angles of 2°, 4.2° and 6.4°. The 4.2° range will allow the 500-700 eV range to be covered with a better throughput than at present while still using the 1200 ℓ mm^{-1} grating. The increased mirror-slit distance reduces the demagnification required and hence the aberrations. The source size limited resolution for the 2° range should then be

achievable. The internal construction of the monochromator lends itself to this mirror changeover modification. The use of spherical optics throughout is a considerable simplification, since aspheric optics of the required precision are difficult to obtain. The beam height at the sample will be significantly reduced to less than 1 mm for all three ranges. The image width should reduce to approximately 1.5 mm with the smaller source size.

The high thermal density on the fused silica grating will continue to be monitored in an attempt to establish a limiting power load for such gratings. The use of the newly developed silicon carbide laminar gratings[22] will be considered once a conclusive result is established.

ACKNOWLEDGEMENTS

The establishment of the Surface EXAFS beamline facility at the Daresbury SRS required the help of many people. We are indebted to D. Tole of Bird and Tole Ltd. for his careful engineering of the monochromator, to W. Smith for the engineering and coordination of the beamline as a whole, to J.-C. Campuzano and R.G. Jones for their perseverance and help during the initial stages of the beamline development and also to R. Brooks, G. Lamble, G. Thornton and I. Owen for their tolerance and useful comments during the use of the beamline for their own studies.

REFERENCES

1. See, e.g., D. Norman, J. Phys. C: Solid State Phys., in press.
2. J. Cerino, J. Stöhr, N. Hower, and R.Z. Bachrach, Nucl. Instrum. Meth. 172, 227 (1980).
3. K.P. Miyake, R. Kato, and M. Yamashita, Sci. Light, 18, 39 (1969).
4. J.B. West, K. Codling, and G. Marr, J. Phys. E: Sci. Instrum. 7, 137 (1974).
5. M.R. Howells, Nucl. Instrum. Meth. 177, 127 (1980).
6. J.A.R. Samson, Techniques of Vacuum Ultra Violet Spectroscopy (Wiley, New York, 1967) p.34.
7. G.M. Miles, Proc. SPIE 315, 65 (1982).
8. J.A. Howell and P. Horowitz, Nucl. Instrum. Meth. 125, 225 (1975).
9. J.B. West, J.-C. Campuzano, and D. Norman, Proc. SPIE 315, 75 (1982).
10. R.P. Walker, Theoretical source size memorandum, SRS/MI/82/17 (1982).
11. Compare this with the JUMBO beamline at SSRL[2], where power loading is about a factor of 10 higher due to the 1° grazing angle and 3.5 GeV running of SSRL.
12. Minilid 310, Heidenhain Ltd., West Germany.
13. Ferranti Astron Ltd., United Kingdom.
14. This arrangement maximises heat dissipation and minimises fabrication difficulties in the carbon films.
15. G.N. Greaves, G.P. Diakun, P.D. Quinn, M. Hart, and D.P. Siddons, Nucl. Instrum. Meth. 208, 335 (1983).
16. Z. Hussain, E. Umbach, D.A. Shirley, J. Stöhr, and J. Feldhaus, Nucl. Instrum. Meth. 195, 115 (1982).
17. B.L. Henke, J.P. Krauer, and K. Premaratne, J. Appl. Phys. 52 (3), 1509 (1981).
18. W.J. Viegele, Atomic Data Tables, 5, 51 (1973).
19. J.W. DuMond, Phys. Rev. 52, 872 (1937).

[20]. T. Ohta, Y. Kitajima, H. Sekiyama, K. Asakura, and H. Kuroda, Photon Factory Activity Report, V1-112 (1983/84).

[21]. G.N. Greaves, P.J. Duke, and R.S. Holt, Daresbury Laboratory DL/SCI/TM27E.

[22]. M. Lewis, Nucl. Instrum. Meth., in press.

[23]. M. Rowen, A. Waldhauer, and P. Planetta, Nucl. Instrum. Meth., in press.

[24]. A.A. MacDowell, J.B. West, and T. Kolde, Nucl. Instrum. Meth., in press.

[25]. W.R. Hunter and R.T. Williams, Nucl. Instrum. Meth. 222, 359 (1984).

[26]. D. Norman, C.H. Richardson, D.R. Warburton, G. Thornton, R. McGrath and F. Sette, to be published.

[27]. D. Norman, F. Setts, A.A. MacDowell and C.H. Richardson, to be published.

[28]. R. McGrath, D.R. Warburton, I.T. McGovern, G. Thornton and D. Norman, submitted to Surf. Sci.

[29]. H.A. Padmore, S.E.M. pictures of gold on float glass mirrors, private communication (1983).

[30]. L.I. Johansson and J. Stöhr, Proc. VI Conference on Vacuum Ultra-violet Radiation Physics, 1980.

[31]. E. Dietz, W. Braun, A.M. Bradshaw, R.L. Johnson, Nucl. Instrum. Meth. 293 (1985) 359.

[32]. J. Stöhr, R. Jaeger, J. Feldhaus, S. Brennan, D. Norman and G. Apai, Appl. Optics 19 (1980) 3911.

[33]. B.E.Warren, X-ray diffraction, Addison-Wesley, Reading, Massachusetts (1969) p.329.

[34]. B.L. Henke, R.C.C. Perera, E.M. Gullikson, M.L. Schattenburg, J. Appl. Phys. 49 (1978) 480.

[35]. J.A. Golovchenko, R.A. Levesque, P.L. Cowan, Rev. Sci. Instrum. 52, 509 (1981).

TABLE I. Parameters of the grating/mirror monochromator based on the Miyake principle[3]. The radiation is collimated as described in the text by a mirror at 11 m from the source. Grating-exit slit distance = 375 mm, vertical displacement of input/output beams = 20 mm. Optics are assumed to be gold coated. Grating to operate in negative order.

Lines/mm	1200		600	
Range	1	2	1	2
Grazing incidence angle at zero order (deg)	2.0	6.4	2.8	6.4
Focusing mirror - exit slit distance (mm)	88	288	88	288
Range of 2nd order reflection filtering (Å)	6.5-15.5	25-52	7-14	25-50
Range of 3rd order reflection filtering (Å)	6.5-23	25-79	7-22	25-77
Grating groove depth (Å)	60		60	
Dispersion at exit slit (Å mm^{-1})	3.33	3.33	6.66	6.66
Source size limited resolution (f.w.h.m.) (Å) (f.w.h.m. source height = 1.2 mm)	0.031	0.100	0.062	0.201

APPENDIX

DuMond Diagrams

In his paper, DuMond[19] describes a useful qualitative pictorial way of viewing the transmission of multiple crystal spectrometers. This has received relatively little attention over the years and so we give here a description of 'DuMond Diagrams' as an aid to the understanding of the +1, -1 double crystal monochromator described in this paper.

The Bragg equation can be described as the locus of points on a λ versus θ plot. For a Ge(111) crystal in first order such a plot is shown in fig.18. The locus of points is in reality broadened by the single rocking curve width as is shown by the magnified insert, in which the more intense the shading the higher the x-ray reflectivity. As an example, the reflectivity of the crystal along the line A using 3.0 Å radiation can be examined by using parallel radiation, rotating the crystal and monitoring the reflected x-ray flux. The result is the single crystal rocking curve as shown in B (fig.18).

For a two crystal monochromator in the +1, -1 configuration, each crystal's reflectivity can be represented on a DuMond diagram (fig.19). Rotating one crystal relative to the other translates the plot horizontally such that x-rays are transmitted by the crystals only when the two plots overlap (Bragg angles are then equal for both crystals). This can be seen more clearly in fig.20, which shows a magnified view of the reflectivities of the two crystals in the region of near superposition.

We first discuss the case of non-absorbing crystals in dynamical diffraction where the reflectivity regions of the crystals can be described simply as lying between the two parallel lines of horizontal width $\Delta\theta_C$

corresponding to the single crystal rocking curve. Rotating crystal B translates its reflectivity function horizontally. The x-ray flux transmitted by the two crystals as a function of the angle of crystal B is the double crystal rocking curve, having FWHM equal to 1.32 $\Delta\theta_C$[33]. The peak transmission is when both reflectivities overlap exactly and the transmitted x-rays are represented by the parallelogram ABCD with a wavelength spread ($\Delta\lambda$) given by

$$\lambda_0(\Delta\theta_{SR} + \Delta\theta_C)\cot\theta_B \qquad (1A)$$

where λ_0 is the working wavelength, θ_B is the Bragg angle and $\Delta\theta_{SR}$ is the angular acceptance of the radiation. For Eq.(1A) to be valid there should be no angular variation of intensity within $\Delta\theta_{SR}$ or any reflectivity variation within $\Delta\theta_C$. For highly perfect crystals and short wavelength x-rays this is a reasonable assumption. Note that the resolution is dependent on the single crystal rocking curve width in the double crystal +1, -1 monochromator.

We now discuss the case for absorbing crystals in the long wavelength region where the reflectivity function within $\Delta\theta_C$ is not a flat topped Darwin shape but is a rounded function. It can be shown that in the limiting case the single crystal rocking curve approaches a Lorentzian shape[34], although a pseudo Gaussian/Lorentzian would probably be a better description for the wavelength range of the monochromator described in this paper. In a double crystal rocking curve measurement the single crystal rocking curve function of crystal A is convolved by transposition with the same function of crystal B. For Lorentzian functions the resulting double crystal rocking curve has a FWHM twice that of the starting Lorentzian function. For Gaussian functions the FWHM of the double crystal rocking

curve increases by 1.414, for Darwin shapes the value is 1.32. This means that the double crystal rocking curve widths measured are an upper limit for the single crystal rocking curve which defines the wavelength resolution. Also the convolution of the two single crystal rocking curves within the parallelogram ABCD (fig.19) at the peak reflectivity (total overlap) results in an effective FWHM $\Delta\theta_C$ smaller than that of the individual single crystal rocking curves. (For two Gaussians the reduction in FWHM is by 0.71.) Given that the radiation has a Gaussian distribution of FWHM $\Delta\theta_{SR}$ the FWHM bandpass $\Delta\lambda$ can be approximated by the quadratic summation

$$\lambda_0(\Delta\theta_{SR}^2 + \Delta\theta_C^2)^{1/2} \cot\theta_B$$

where $\Delta\theta_C$ is the FWHM of the double crystal rocking curve, which, from the above discussion represents the upper limit for the contributing angular term.

Another property of double crystal (+1, -1) monochromators can readily be seen from fig.19. The double crystal rocking curve width is independent of the divergence of the polychromatic synchrotron radiation. No apertures are necessary when carrying out such measurements.

The effect of heating on one crystal is to increase the d spacing and consequent displacement on the DuMond diagram. This gives a different gradient for each crystal's reflectivity function (fig.21). There is little effect on the width of the single crystal rocking curve. It can be seen that rotating one crystal relative to the other results in a broader double crystal rocking curve because there is now a contribution from the angular width of the radiation ($\Delta\theta_{SR}$). The effect becomes most significant when $\Delta\theta_{SR}$ is much larger than the single crystal rocking curve width.

Fig. 8 shows the broadening effect on double crystal rocking curves by heating one crystal. The broadening is relatively the largest for the narrowest rocking curves (small Bragg angles) because the angular convergence of the radiation through the monochromator is then relatively large compared to the rocking curve width. Also Ge(111) does not show the effect as much as Ge(220) crystals because the former has the larger rocking curve width. Note that the effect on wavelength resolution is minimal as the resolution is still determined by the single crystal rocking curve.

There is also a reduction in the maximum x-ray intensity reflected as indicated by the shaded hexagonal area (AEFCGH) when compared to the parallelogram (ABCD).

FIGURE CAPTIONS

Fig.1 Optical layout of the beamline. (a) Optical layout with the monochromator in the double crystal mode. The toroidal premirror is bent to focus in both vertical and horizontal planes onto the sample. (b) Optical layout with the monochromator in the grating mode. The toroidal premirror is partially bent to provide parallel radiation for the plane grating in the vertical plane. The premirror focuses through the monochromator to the sample in the horizontal plane.

Fig.2 Schematic diagram of the mirror bending mechanism. The mirror is supported on its base at its two ends. By pulling down on the central rod a downward force can be exerted on the four aluminium pads which sit on the mirror's top outer rim 6 cm in from the end. This results in the required opposing couples that bend the mirror to the required toroidal shape.

Fig.3 Schematic diagram of the monochromator.

Fig.4 Schematic diagram of the beam monitoring section after the monochromator.

Fig.5 Transmission function of InSb(111) crystals. Absolute photon fluxes are calculated using the 0.75 μm thick oxidized aluminium I_0 monitor and the photoemission yield of Al_2O_3[17].

Fig.6 Transmission function of Ge(111) crystals.

Fig.7 Transmission function of Ge(220) crystals.

Fig.8 Measured f.w.h.m. (1, -1) rocking curves as a function of Bragg angle for InSb(111), Ge(111) and Ge(220). The bold lines are for rocking curves under low thermal load. The dashed lines are for rocking curves of Ge(111) and Ge(220) under high thermal load - normal operating conditions (SRS at 2.0 GeV, 250 mA). The InSb(111) rocking curve under high thermal load was not recorded due to surface melting of the first crystal as noted in section V.B.

Fig.9 Calculated resolutions (f.w.h.m.) for the crystals InSb(111), Ge(111) and Ge(220). The solid lines (denoted by C + S + SR) take into account source size, angular convergence of the radiation through the monochromator and crystal rocking curves. This represents the resolution under normal operating conditions. The dashed lines (C + S) represent the resolution that can be obtained when considering only the crystal rocking curves and source height. In this case the radiation is collimated by the premirror such that the crystals see parallel radiation. The solid line (C) is the calculated resolution when considering only the double crystal rocking curve.

Fig.10 Transmission spectrum of the titanium K edge, using Ge(220) crystals in the monochromator, showing the difference in resolution when (full line) the mirror is fully bent - large angular convergence (calculated ΔE = 9.0 eV) and (dashed line) the mirror is bent to produce parallel radiation through the monochromator (calculated ΔE = 2.4 eV). Note that the energy calibration shifts between the two measurements owing to changes in the incident power density on the first monochromator crystal.

Fig.11 Schematic diagram showing the difference in beam paths for the double crystal monochromator with the first crystal hot and cold. The first crystal has to be rotated through a small angle β from the true parallel/parallel θ_D angle when it increases its temperature.

Fig.12 Surface EXAFS spectrum of the sulphur K edge for a 0.5 monolayer coverage of sulphur on a nickel (110) surface, measured by taking the yield of S KLL Auger electrons.

Fig.13 Modulus of the Fourier transforms of EXAFS spectra from a GaS single crystal measured at (a) the S K-edge and (b) the Ga K-edge, with the polarisation vector parallel (full line) and 20° from perpendicular (dashed line) to the surface. The distance scale has not been corrected for the scattering phase-shifts. The main peak is due to the Ga-S nearest neighbours at 2.30 Å, with an additional contribution in (b) from the Ga-Ga neighbours at 2.52 Å, which is not seen with normal incidence photons.

Fig.14 SEXAFS spectrum above the Si K-edge for H^+ ions desorbed from a water-dosed Si(100) surface.

Fig.15 Transmission function of the low energy grating/mirror (6.4°), for 0.1 Å bandpass. Insert figures refer to resolution in eV. Source size limited resolution achieved = 0.07 Å.

Fig.16 Transmission function of the high energy grating/mirror (2°), for 0.1 Å bandpass. Insert figures refer to resolution in eV. Source size limited resolution achieved = 0.04 Å.

Fig.17 Total electron yield from an aluminium alloy (Dural) sample as the low energy grating (6.4°) is scanned through the calcium $2p_{1/2,3/2}$ edges.

Fig.18 The DuMond diagram for a Ge(111) crystal in first order. The reflectivity of the crystal is shown as the locus of points satisfying the Bragg equation. The locus of points is broadened as shown in the magnified insert. Moving across the line A at 3.0 Å results in single crystal rocking curve B.

Fig.19 DuMond diagram representation of the transmission function of each crystal in the +1, -1 non dispersive double crystal monochromator. The rotation of one crystal relative to the other results in a horizontal displacement in the DuMond diagram.

Fig.20 DuMond diagram for the two crystals in the +1, -1 configuration near superposition. The rotation of crystal B translates its reflectivity function over that of crystal A. Maximum x-ray flux is transmitted at total overlap. The transmitted x-ray intensity is indicated by the area of the parallelogram AECD.

Fig.21 DuMond diagram for maximum reflectivity of +1, -1 double crystal monochromator for one hot and one cold crystal. The area AEFCGH represents the reflected x-ray intensity which is smaller than the area ABCD which represents the cold-cold crystal reflectivity.

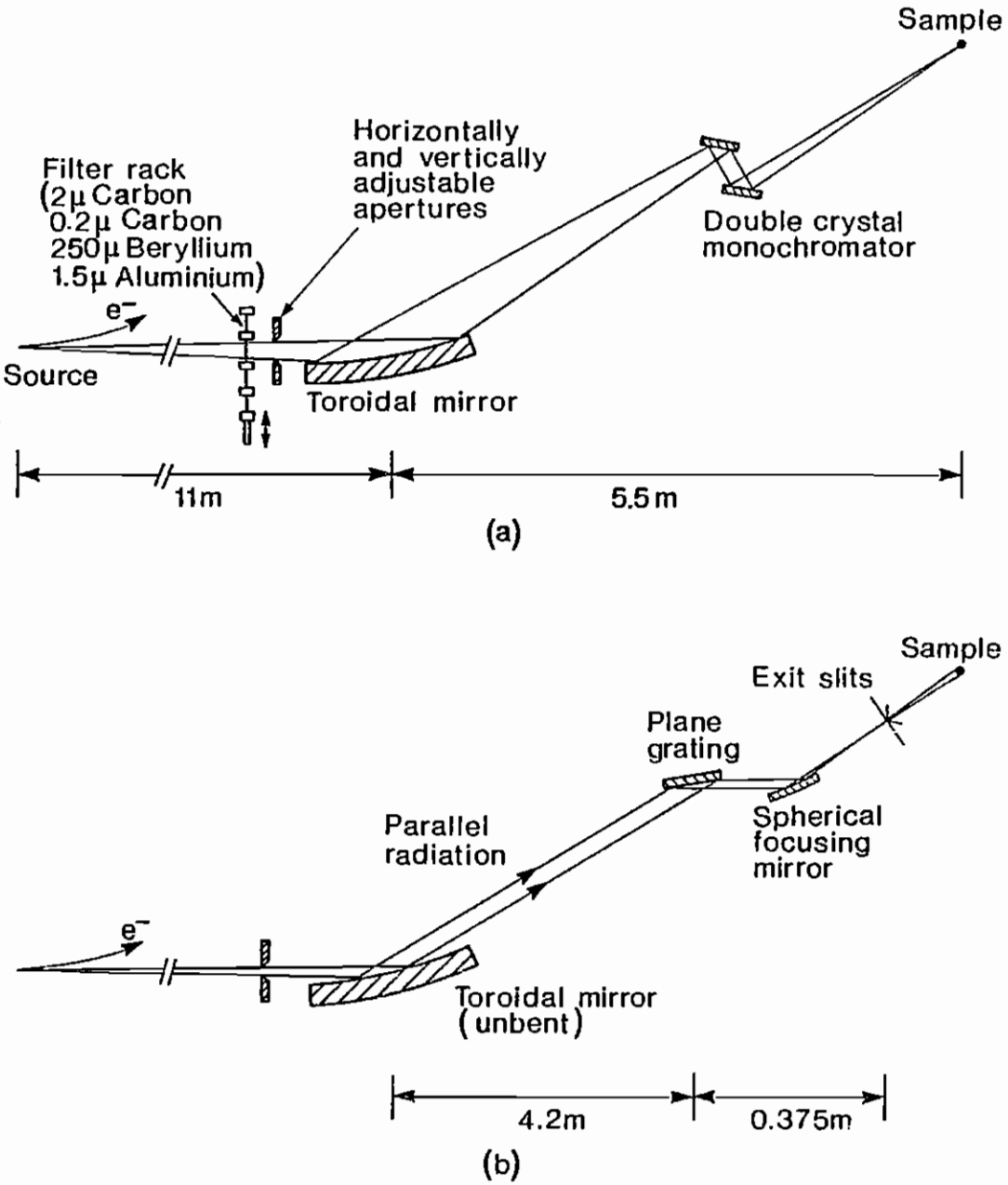
Sample
Horizontally
and vertically
adjustable
apertures
Filter rack
(2μ Carbon
0.2μ Carbon
250μ Beryllium
1.5μ Aluminium)
Double crystal
monochromator
e⁻
Source
Toroidal mirror
11m
5.5m
(a)
Sample
Exit slits
Plane
grating
Parallel
radiation
Spherical
focusing
mirror
e⁻
Toroidal mirror
(unbent)
4.2m
0.375m
(b)

Fig. 1

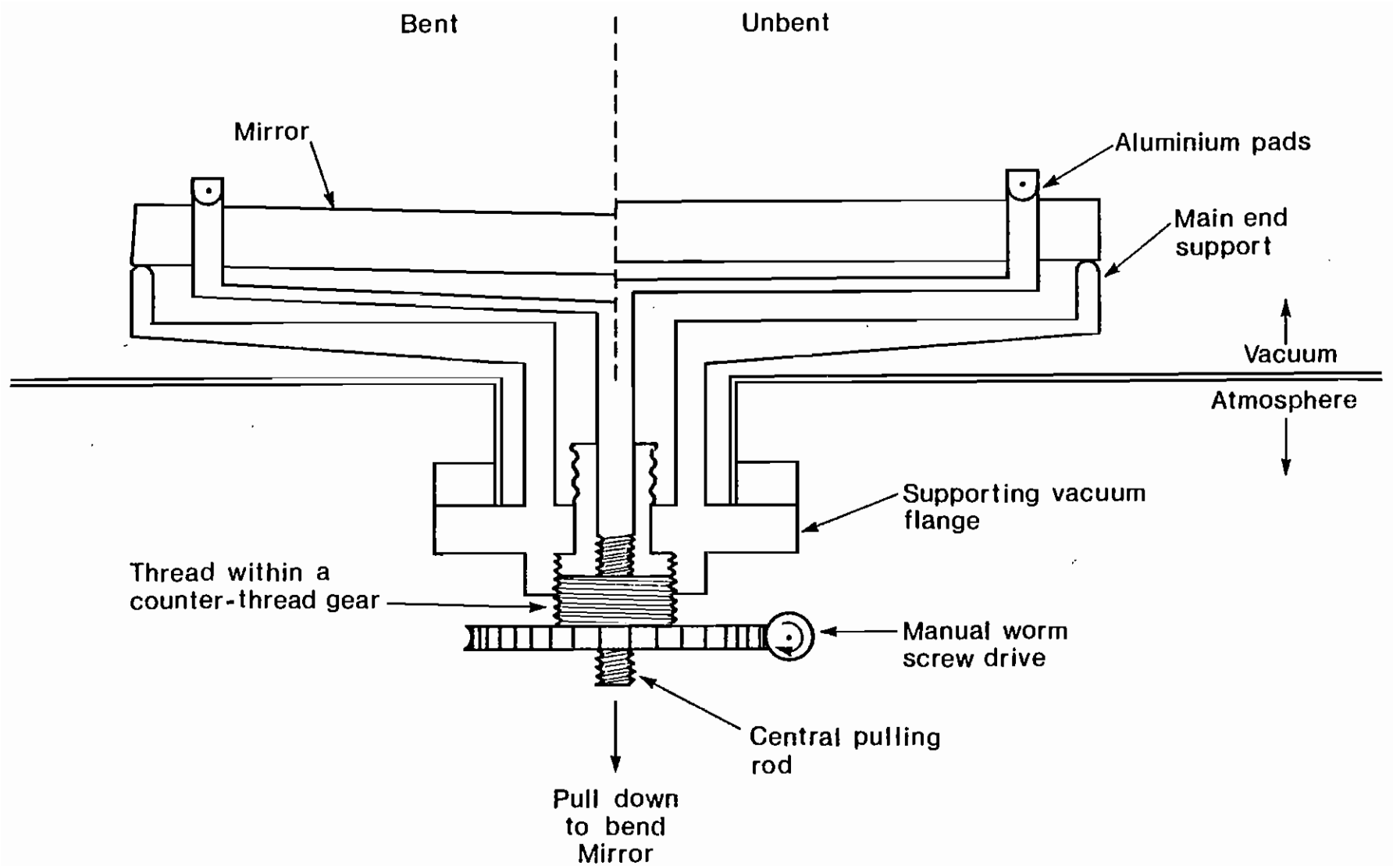
Bent
Unbent
Mirror
Aluminium pads
Main end support
Vacuum
Atmosphere
Supporting vacuum flange
Thread within a counter-thread gear
Manual worm screw drive
Central pulling rod
Pull down to bend Mirror

Fig. 2

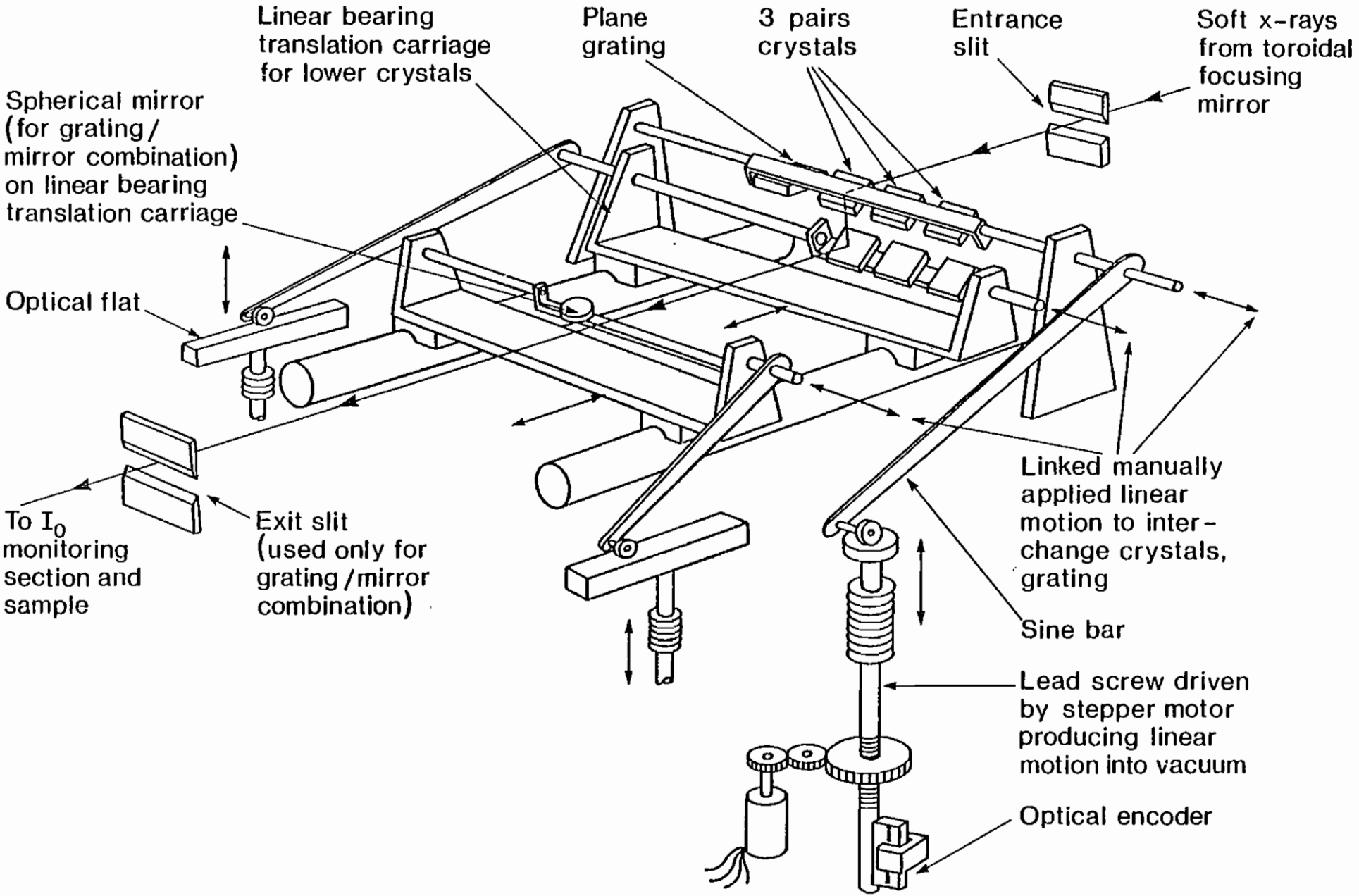
Linear bearing translation carriage for lower crystals
Plane grating
3 pairs crystals
Entrance slit
Soft x-rays from toroidal focusing mirror
Spherical mirror (for grating/ mirror combination) on linear bearing translation carriage
Optical flat
To I_0 monitoring section and sample
Exit slit (used only for grating/mirror combination)
Linked manually applied linear motion to inter-change crystals, grating
Sine bar
Lead screw driven by stepper motor producing linear motion into vacuum
Optical encoder

Fig. 3

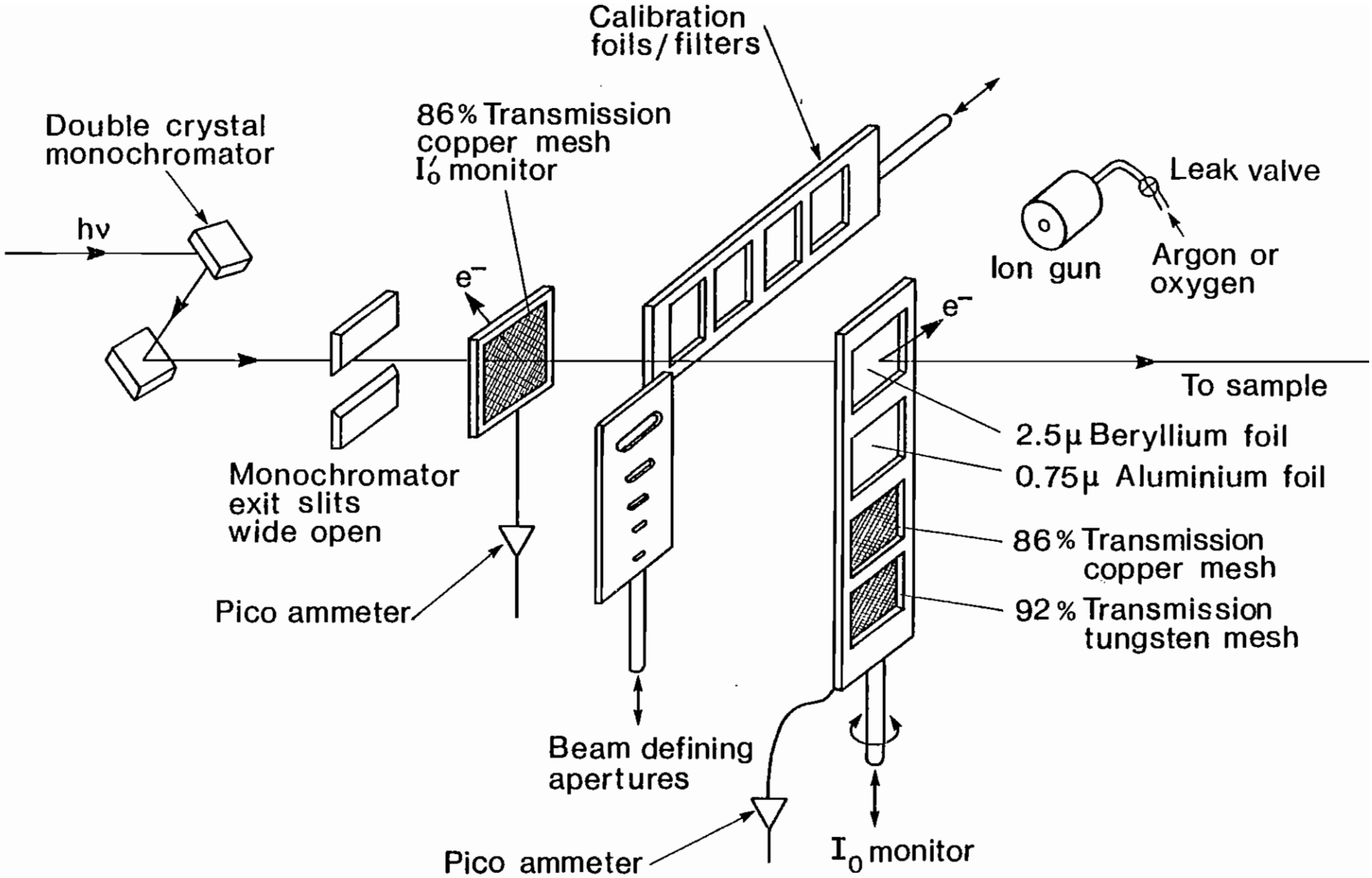
Calibration
foils/filters
Double crystal
monochromator
86% Transmission
copper mesh
I_o' monitor
Leak valve
hν
e⁻
Ion gun
Argon or
oxygen
e⁻
To sample
2.5μ Beryllium foil
0.75μ Aluminium foil
Monochromator
exit slits
wide open
86% Transmission
copper mesh
Pico ammeter
92% Transmission
tungsten mesh
Beam defining
apertures
Pico ammeter
I_0 monitor

Fig. 4

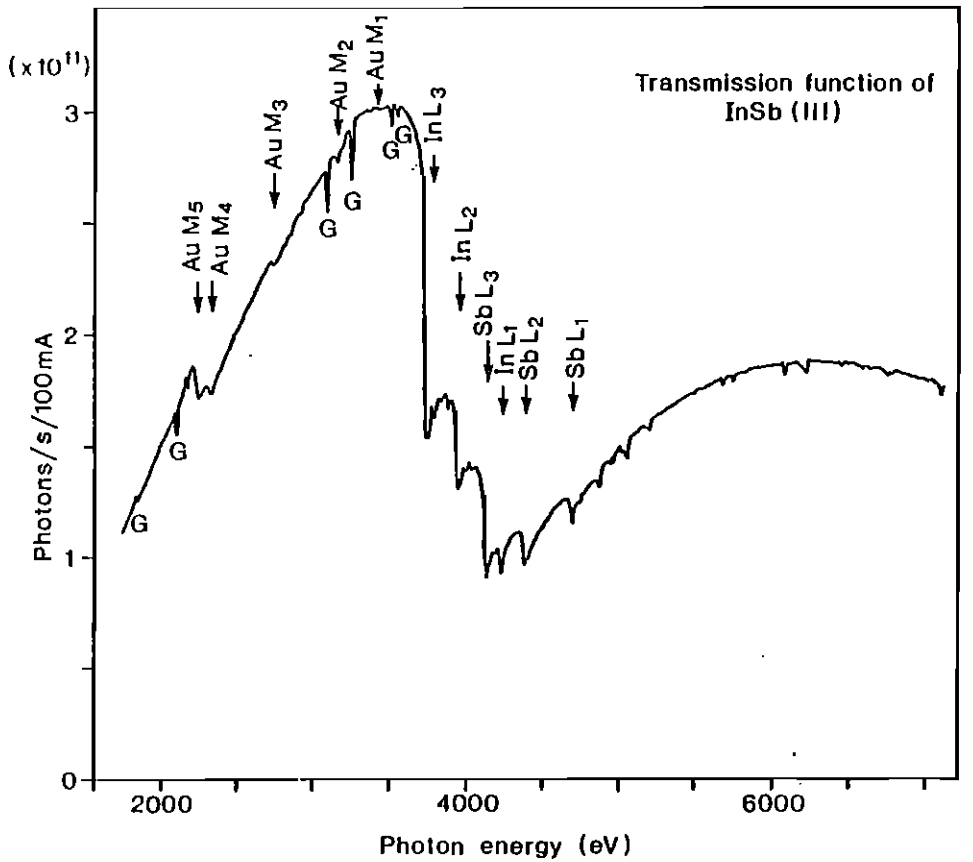
(x10^11)
Photons/s/100mA
Transmission function of
InSb (111)
Au M5
Au M4
Au M3
Au M2
Au M1
In L3
In L2
Sb L3
In L1
Sb L2
Sb L1
G
Photon energy (eV)

Fig. 5

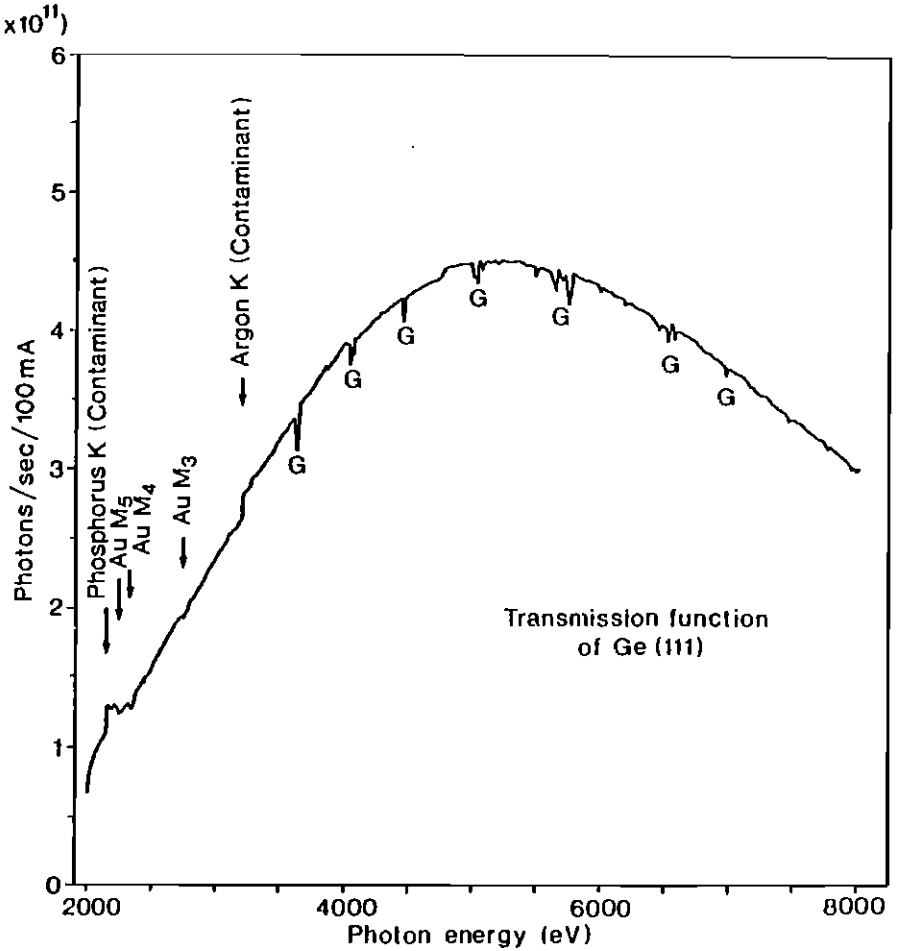
(x10^11)
Photons/sec/100mA
Phosphorus K (Contaminant)
Au M5
Au M4
Au M3
Argon K (Contaminant)
Transmission function
of Ge (111)
G
Photon energy (eV)

Fig. 6

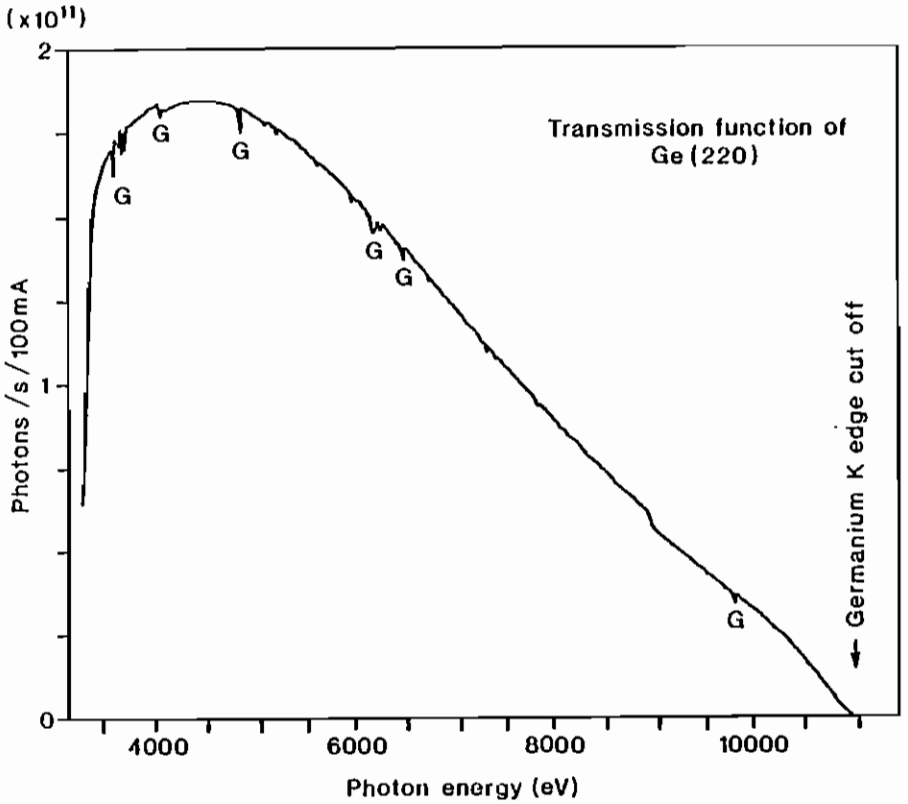
(x10^11)
2
1
0
Photons /s/100mA
Transmission function of
Ge(220)
G
G
G
G
G
G
Germanium K edge cut off
4000
6000
8000
10000
Photon energy (eV)

Fig. 7

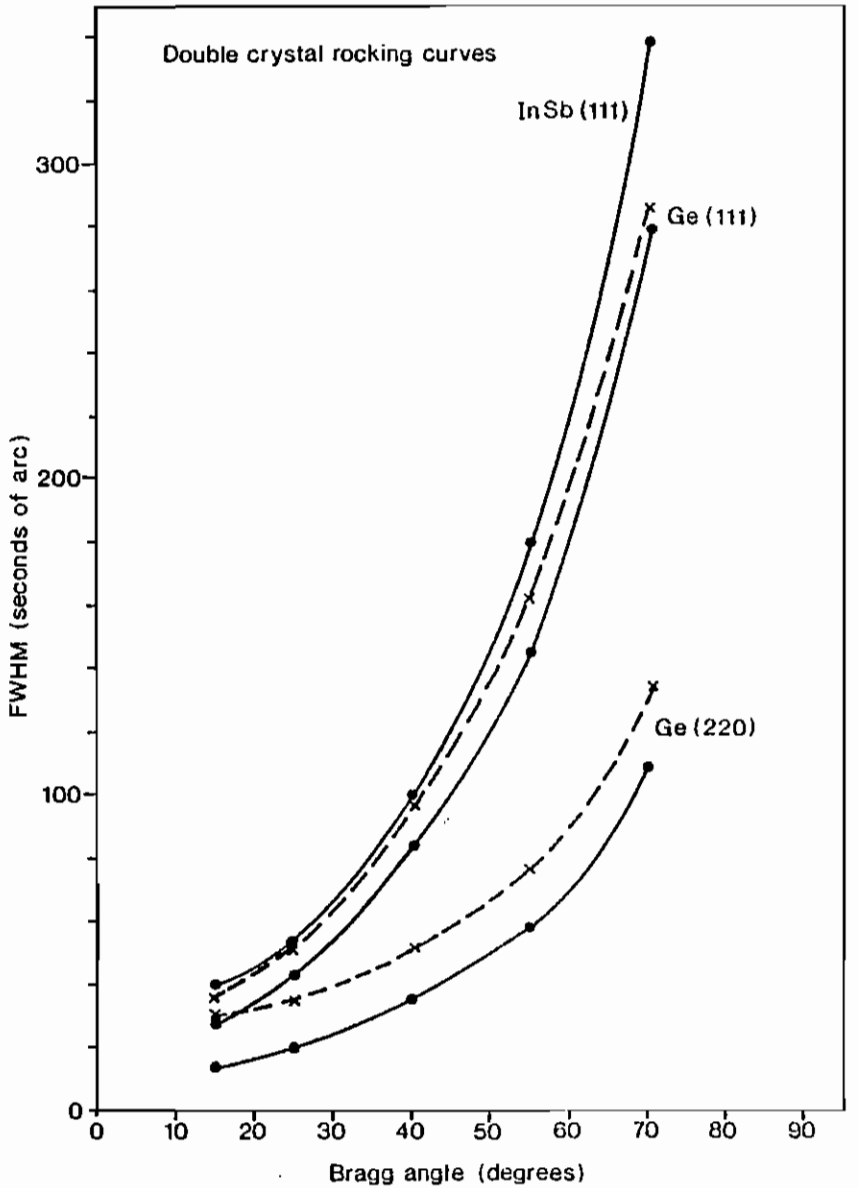
Double crystal rocking curves
InSb (111)
Ge (111)
Ge (220)
300
200
100
0
FWHM (seconds of arc)
0
10
20
30
40
50
60
70
80
90
Bragg angle (degrees)

Fig. 8

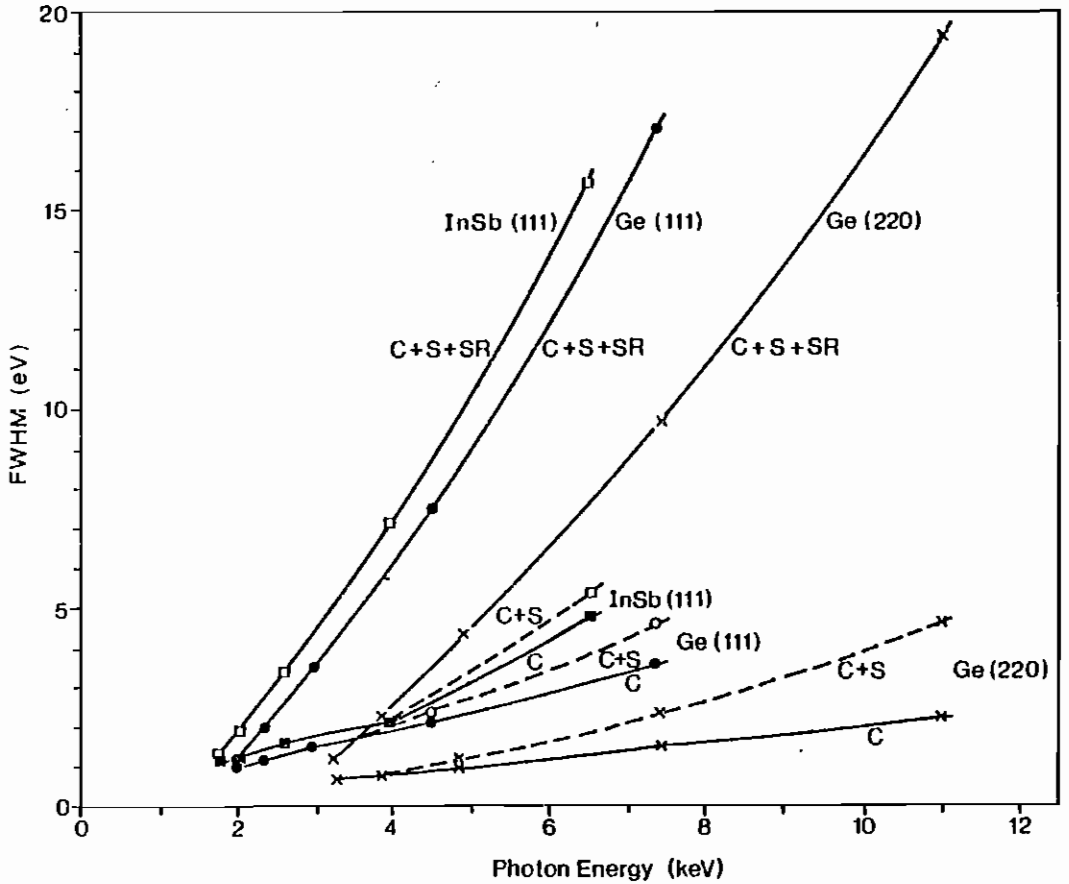
FWHM (eV)
Photon Energy (keV)
InSb (111)
Ge (111)
Ge (220)
C+S+SR
C+S+SR
C+S+SR
C+S
InSb (111)
C
C+S
Ge (111)
C
C+S
Ge (220)
C

Fig. 9

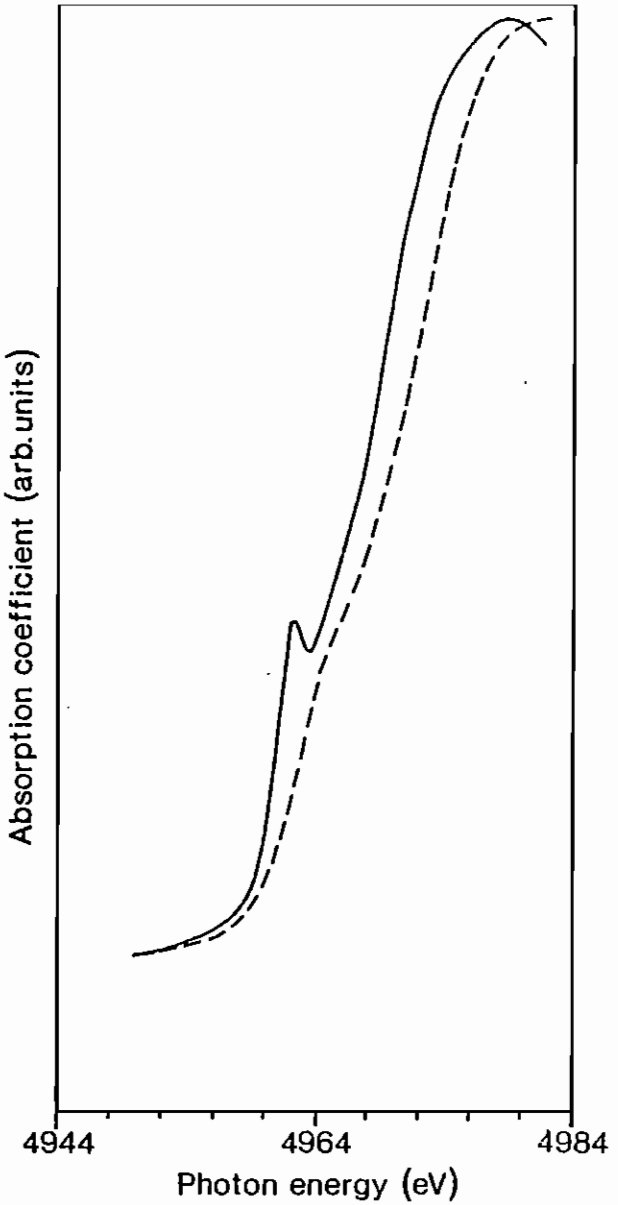
Absorption coefficient (arb.units)
4944
4964
4984
Photon energy (eV)

Fig. 10

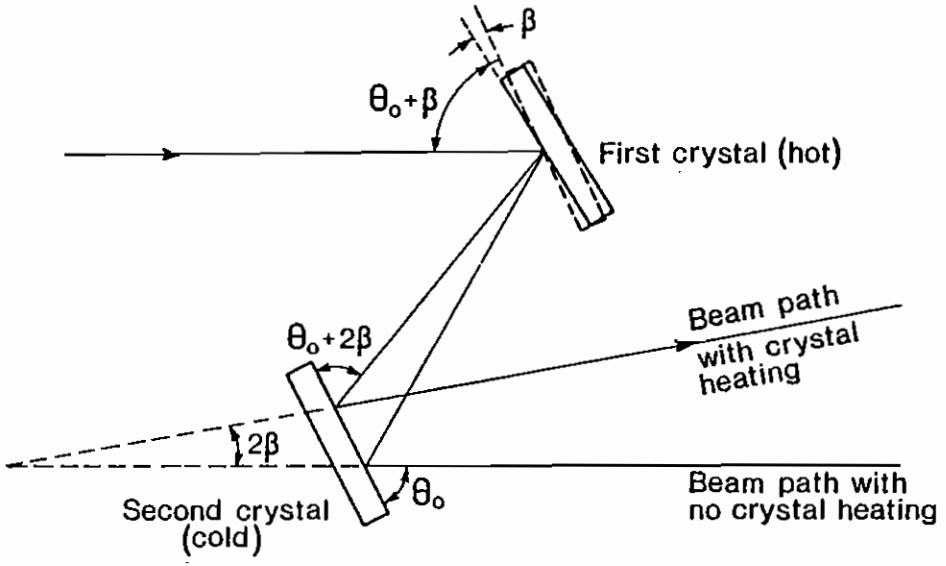
β
θo+β
First crystal (hot)
θo+2β
Beam path
with crystal
heating
2β
θo
Second crystal
(cold)
Beam path with
no crystal heating

Fig. 11

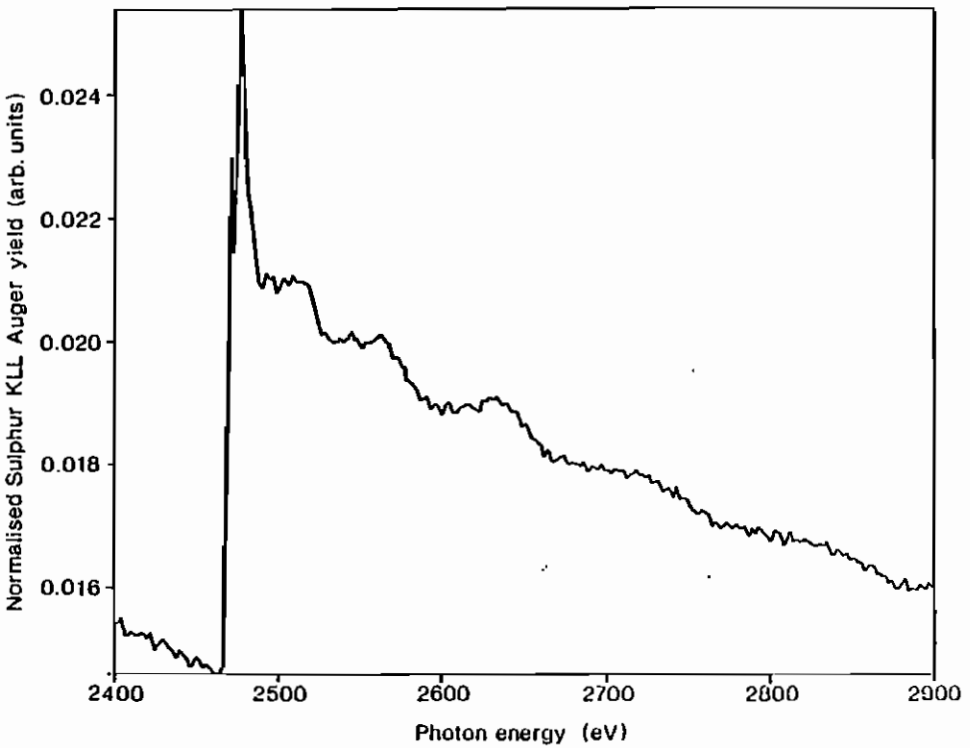
Normalised Sulphur KLL Auger yield (arb. units)
0.024
0.022
0.020
0.018
0.016
2400
2500
2600
2700
2800
2900
Photon energy (eV)

Fig. 12

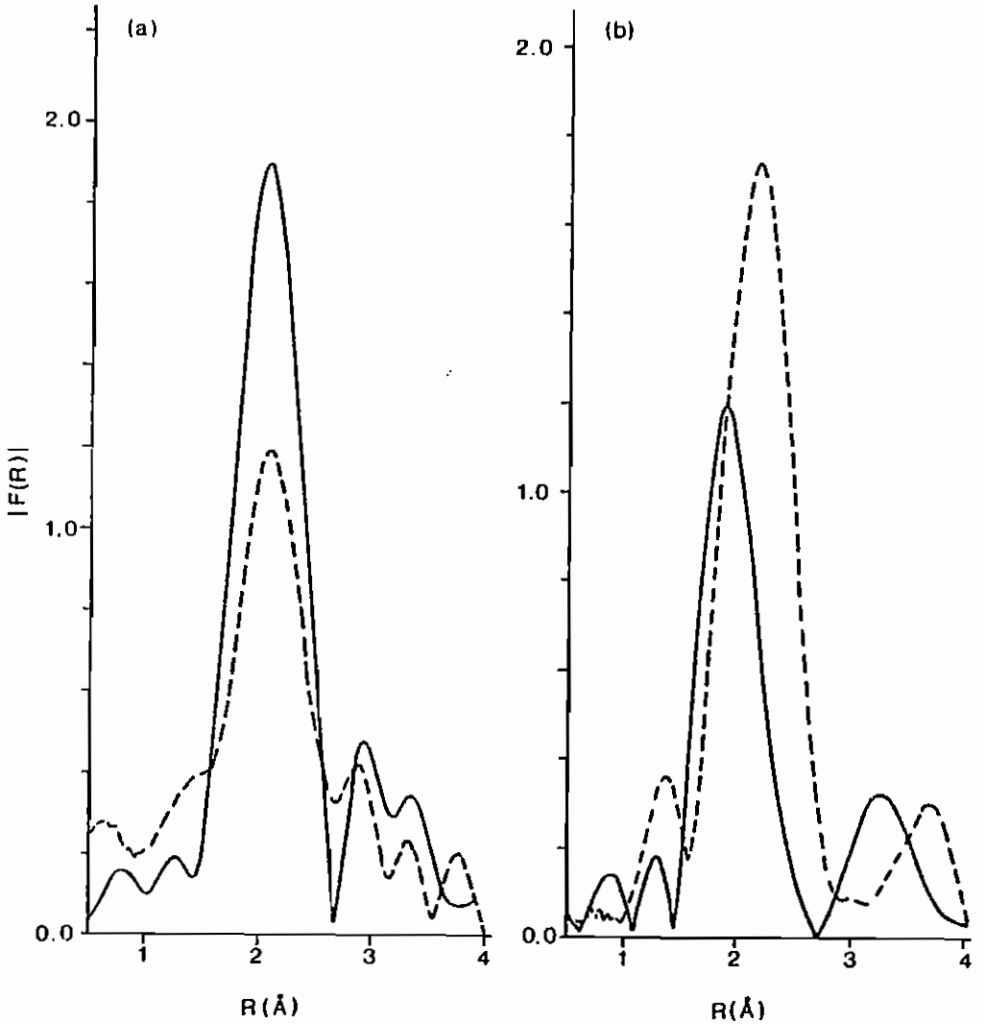
(a)
(b)
2.0
1.0
0.0
|F(R)|
1
2
3
4
R(Å)

Fig. 13

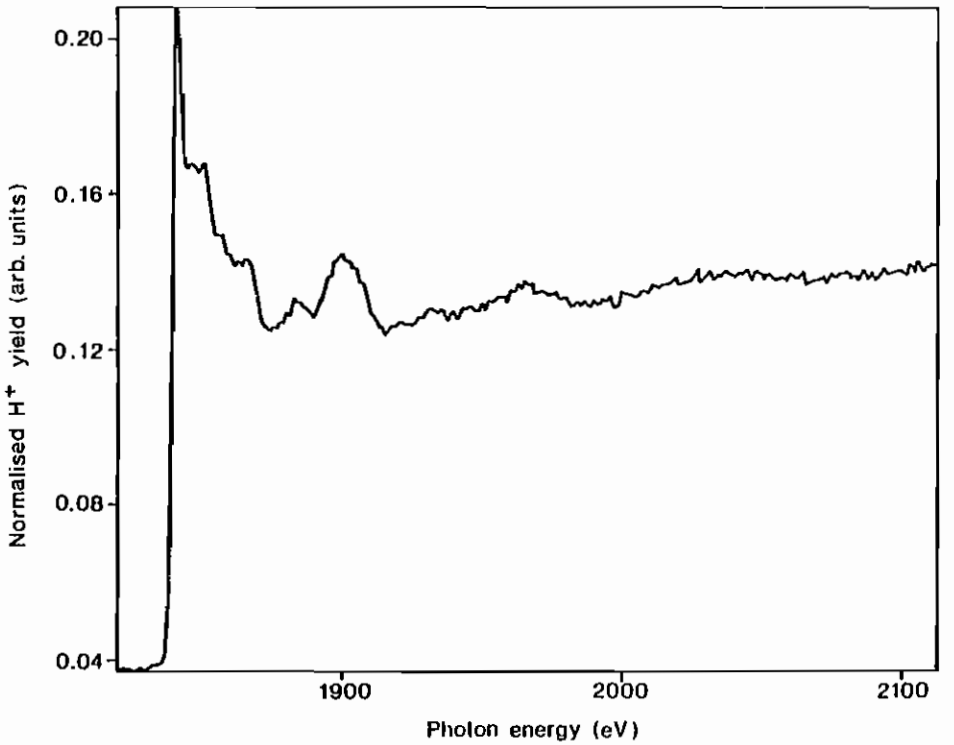
0.20
0.16
0.12
0.08
0.04
Normalised H+ yield (arb. units)
1900
2000
2100
Photon energy (eV)

Fig. 14

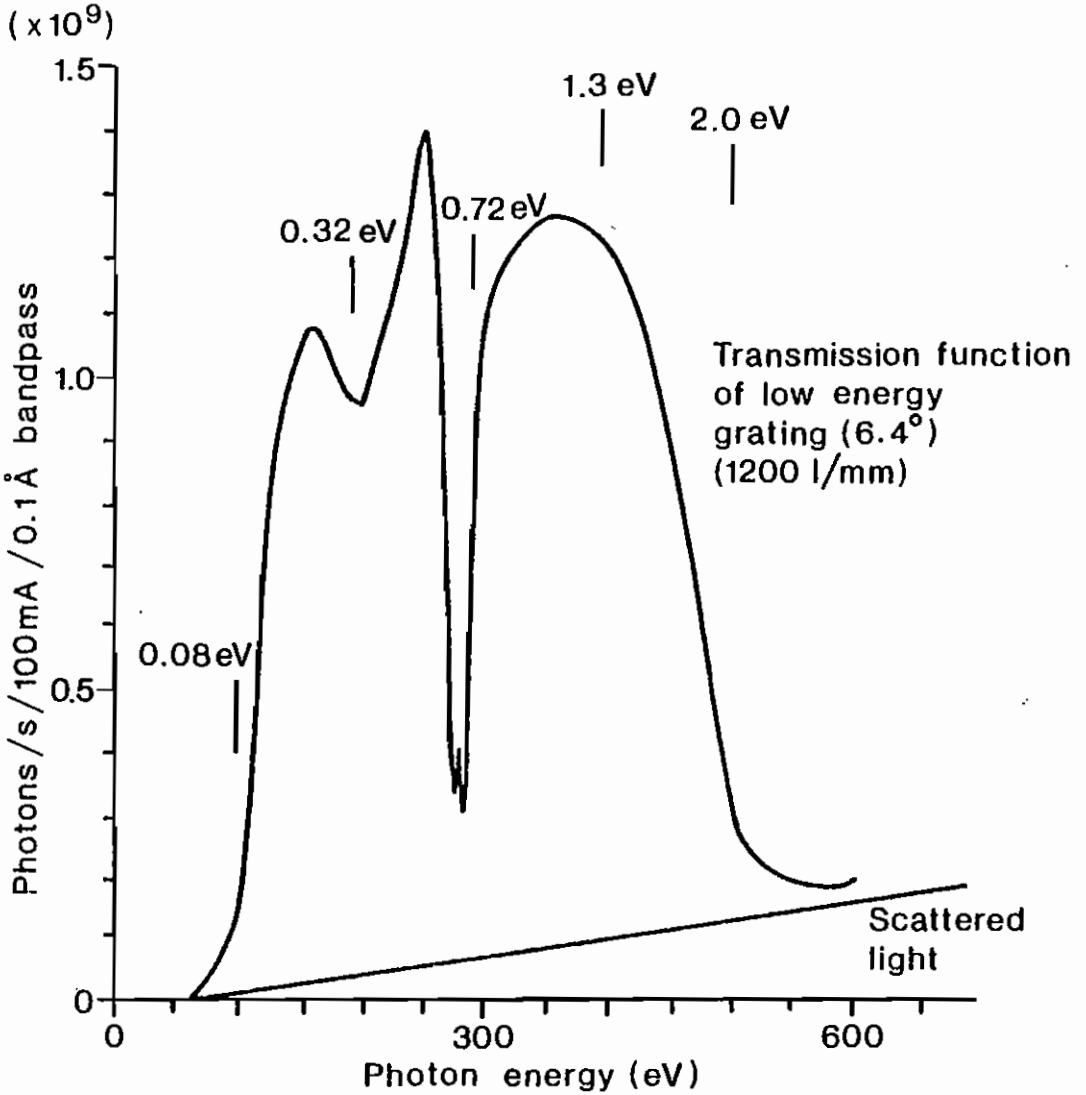
(x10^9)
1.5
1.0
0.5
0
Photons/s/100mA/0.1Å bandpass
0.08 eV
0.32 eV
0.72 eV
1.3 eV
2.0 eV
Transmission function of low energy grating (6.4°) (1200 l/mm)
Scattered light
0
300
600
Photon energy (eV)

Fig. 15

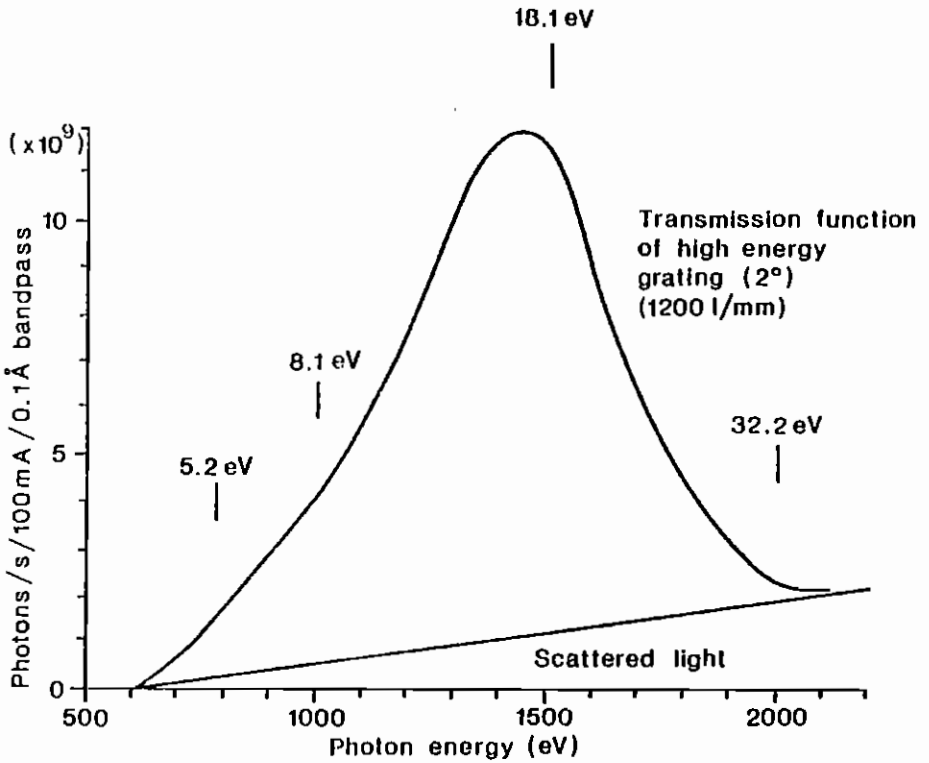
18.1 eV
(x10^9)
Photons/s/100mA/0.1Å bandpass
10
5
0
8.1 eV
5.2 eV
32.2 eV
Transmission function
of high energy
grating (2°)
(1200 l/mm)
Scattered light
500
1000
1500
2000
Photon energy (eV)

Fig. 16

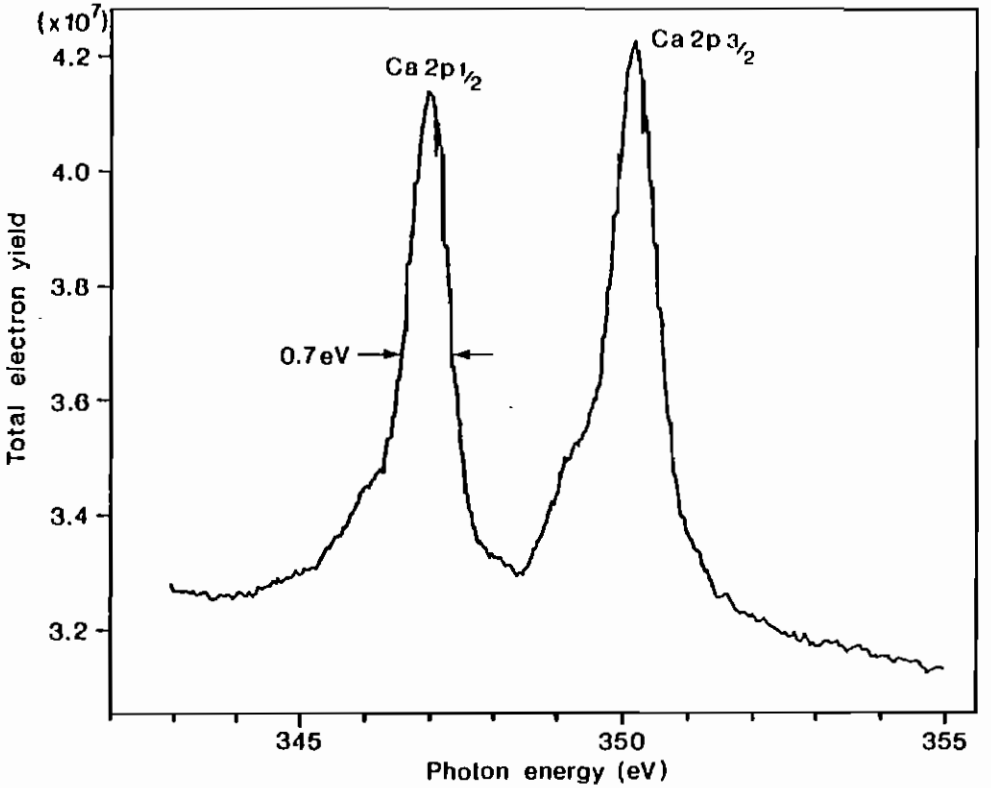
(x10^7)
Total electron yield
4.2
4.0
3.8
3.6
3.4
3.2
Ca 2p 1/2
Ca 2p 3/2
0.7 eV
345
350
355
Photon energy (eV)

Fig. 17

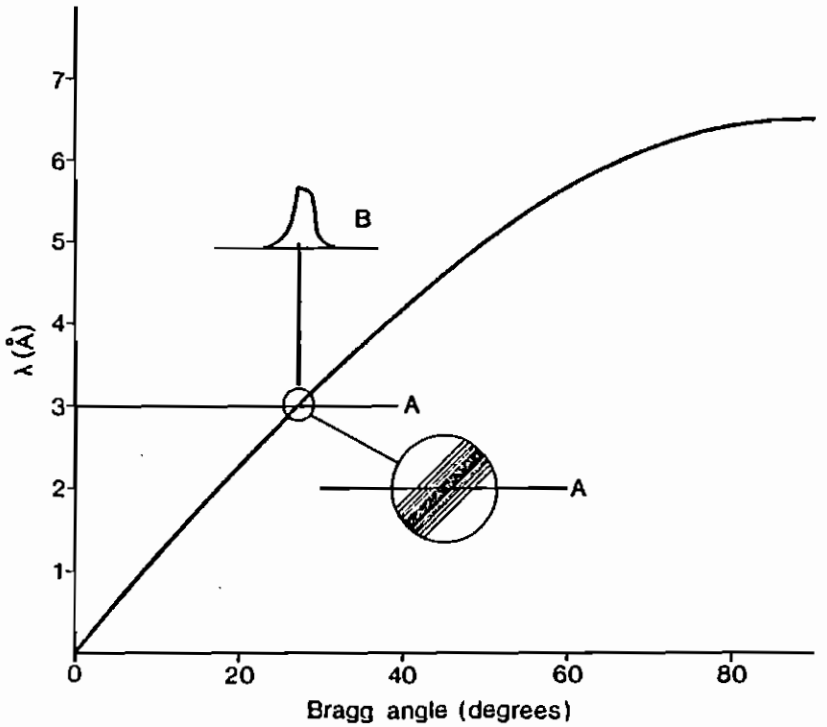
7
6
5
4
3
2
1
λ (Å)
B
A
A
0
20
40
60
80
Bragg angle (degrees)

Fig.18

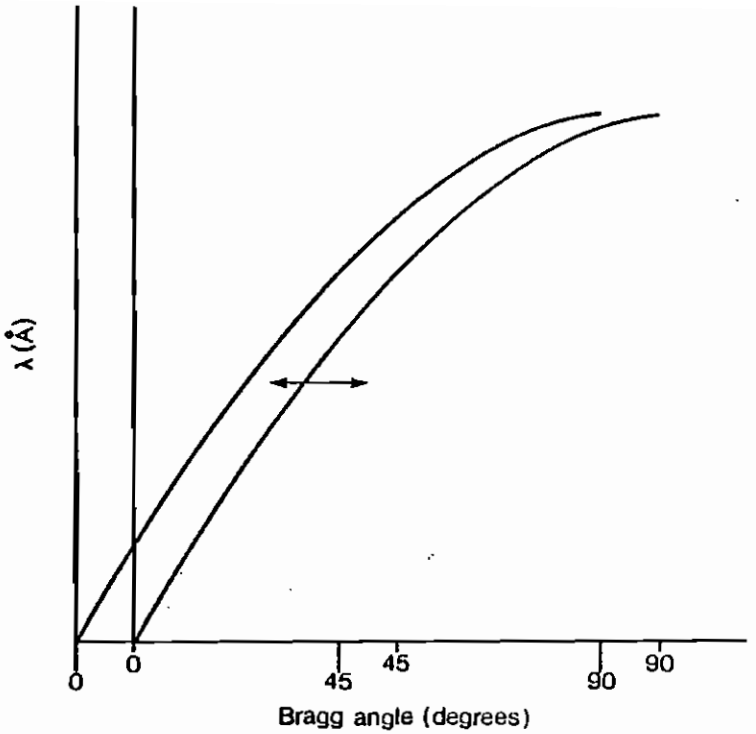
λ (Å)
0
0
45
45
90
90
Bragg angle (degrees)

Fig.19

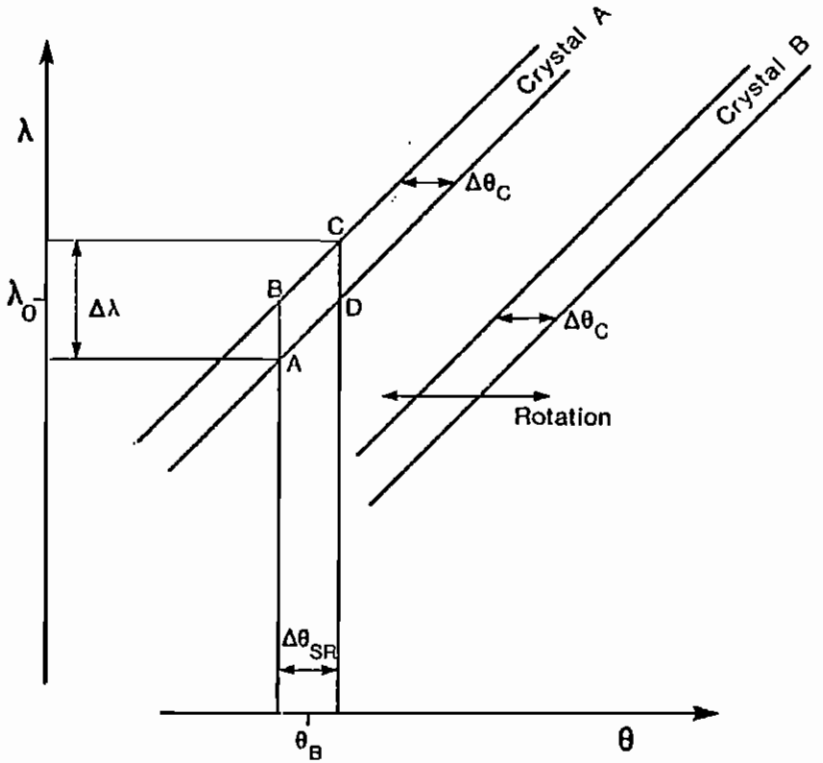
λ
λ0
Δλ
Crystal A
Crystal B
Δθc
Δθc
C
B
D
A
Rotation
ΔθSR
θB
θ

Fig. 20

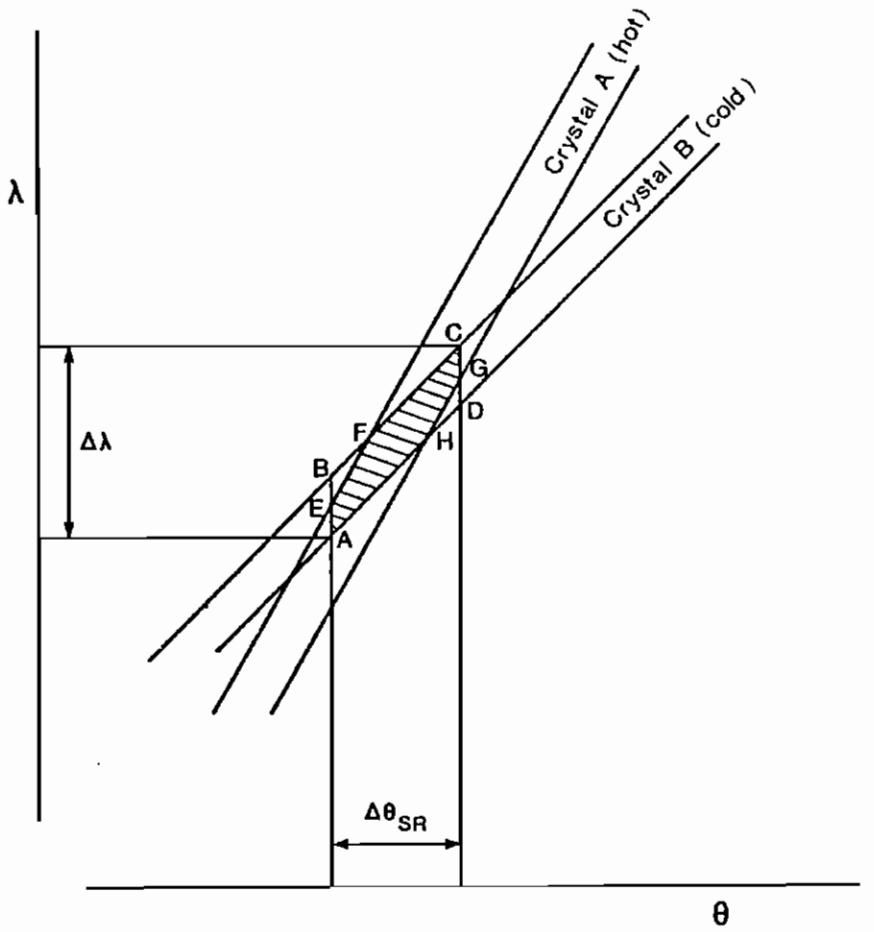
λ
Crystal A (hot)
Crystal B (cold)
C
G
D
F
H
Δλ
B
E
A
ΔθSR
θ

Fig. 21